Georgia Institute of Technology

Final Report

Titled

"EN ROUTE JET AIRCRAFT NOISE ANALYSIS"

DELIVERABLE NO. 3

Submitted to:

Dr. Hua (Bill) He
Federal Aviation Administration
AEE-100
800 Independence Avenue SW
Washington DC 20591

Prepared by:

Aerospace Systems Design Laboratory
School of Aerospace Engineering
Georgia Institute of Technology
Atlanta, GA 30332

December 15, 2012

Principal Investigator:
Professor Dimitri N. Mavris
Director, Aerospace Systems Design Lab
Boeing Professor,
Advanced Aerospace Systems Analysis
School of Aerospace Engineering
Georgia Institute of Technology
Tel: 404-894-1557
Fax: 404-894-6596
Email: dimitri.mavris@ae.gatech.edu

Co-Principal Investigator:
Jimmy Tai, Ph.D.
Division Chief
ASDL Propulsion & Energy Division
Senior Research Engineer
School of Aerospace Engineering
Georgia Institute of Technology
Tel: 404-894-0197
Fax: 404-894-6596
Email: jimmy.tai@ae.gatech.edu

Table of Contents

Table of Figures

Table of Figures

1.0 Background and Problem Formulation

Most research into commercial noise is primarily focused on reducing the community noise, noise that the local population near an airport experiences as aircraft takeoff and land. While this type of noise may be a main driver for the noise that communities experience, noise generated by an aircraft during climb, cruise, and descent segments of flight might also reach the ground and affect the noise level experienced by these communities. The noise from these sources can have the same annoying effects as those experienced during takeoff and landing. En route noise can become problematic and produce similar annoyance as that experienced near airports when aircraft are flying over rural areas. These areas have a lower ambient noise level than that of cites, and the noise generated by the aircraft will not be easily masked by that of other transportation modes. National Parks within rural areas are prime examples where the effects of en route noise may become significant. National Parks have an ambient noise level even lower than rural areas, and hence, the low frequency noise that is propagating from an aircraft overhead could have an adverse effect upon the wildlife within the park, as well as any visitors. There are numerous research efforts currently being funded to predict the propagation of en route noise to the ground, but the available prediction methods for the noise sources are unfortunately limited. This limitation exists because most noise prediction codes were created and validated on noise generated at low-altitude conditions, such as takeoff and landing.

1.1 Problem Definition

The research documented in this interim report will start to address the research gap in predicting en route noise sources by leveraging existing modeling capability. The objective of this research is to develop a prediction capability in Aircraft Environmental Design Tool (AEDT) for the far-field source noise generated by en route aircraft.

1.2 Environmental Design Space (EDS) Description

EDS is an aircraft modeling and simulation tool capable of predicting the fuel burn, NOx emissions, and noise metrics in a single environment with an automated link to provide necessary data for a fleet level assessment. EDS is capable of modeling the thermodynamic performance of any engine cycle using NASA's Numerical Propulsion System Simulation (NPSS) [1,2] coupled with a parametric component map generation tool (NASA's CMPGEN [3]) and with a 1-D aeromechanical design/analysis for flowpath and weight estimation purposes (NASA's WATE++ [4]). This propulsion system simulation is well suited to assess engine performance and is also very unique because it employs a simultaneous, multi-design point sizing algorithm develop by ASDL [5]. The propulsion simulation module is coupled with the mission analysis module (NASA's FLOPS [6]) in an iterative fashion to ensure that all coupling variables are internally consistent and have converged. EDS ensures convergence and consistency in order to provide more accurate fuel burn results and more accurate data to the noise prediction module (NASA's ANOPP [7,8]) to assess acoustic impacts. Another important module in EDS is the NOx prediction algorithm which uses correlations developed from a combined 1-D combustor geometric model and a chemical reaction network model. Finally, EDS is well suited to be coupled to a fleet level analysis since it has an automated process to

generate the vehicle/engine/noise information and/or coefficients necessary to provide replacement aircraft. EDS has been, or is being, successfully used in support of several projects including:

- FAA CLEEN Program: Aircraft and fleet level technology modeling and assessment
- ACRP 2-27 Aircraft Taxi Noise Database for INM and AEDT: EDS noise-power-distance curves were used to support the prediction of taxi noise
- NASA ERA: Ongoing system analysis support for the ERA technology portfolio assessment for advanced concepts
- NASA SFW: Supports advancing the fundamental analytical concepts of EDS with higher fidelity emissions, open rotor performance and noise, and also provides N+3 modeling capabilities such as distributed propulsion and hybrid wing body capability
- Interagency Portfolio Systems Analysis (IPSA): Providing future replacement vehicle definitions for fleet level assessments
- Joint Planning Development Office Technology Standing Committee (JPDO TSC): Supporting the technology roadmap definitions through a screening tool analysis
- FAA ATO Office: Assessing the implications of CO_2 metrics for US policy analysis for varying future fleet scenarios
- ICAO/CAEP: Supported the CAEP/9 noise stringency analysis
- EPA: Assessing the cost-benefit of imposing a CO_2 standard on total CO_2 standard at what cost to manufacturers

Since the original intent of EDS was to support the CAEP process, it was initially created under intense scrutiny. In 2005-2006 a Technical Advisory Board (TAB) and later in 2007, an international Independent Review Group (IRG) was formed to evaluate and assess EDS for use in CAEP. The IRG consisted of NASA and industry members and performed an in depth review of all of the assumptions inherent within EDS. The IRG came to an agreement on the underlying data and assumptions used to establish the design space of the EDS 777-200ER model with both Pratt and Whitney and General Electric engines. The IRG also reviews the EDS 737-800 and CRJ900 models. In 2008 the FAA redirected the development focus of EDS to be NextGen centric and the IRG ceased. However, with continued FAA support of EDS, the vehicle library continued to expand, and at present contains 7 vehicle models that can, and are, being used for analysis work. These vehicles are shown in Table 1 below:

Table 1: EDS Calibrated Models

Vehicle Size	Aircraft Model	Engine Model
Regional Jet	ERJ190	CF34-10
Regional Jet	CRJ-900	CF34-8C5
Single Aisle	Boeing 737-800	CFM56-7B27
Small Twin Aisle	Boeing 767-300ER	CF6-80C2
Large Twin Aisle	Boeing 777-200ER	GE90-94B
Very Large Twin	Boeing 747-400	PW4060

These baseline EDS vehicles were created using the same calibration process developed and reviewed by the IRG. This calibration process begins with gathering detailed public domain information on these models from sources including:

- ICAO emissions data bank
- Jane's Aero-Engines
- Jane's All the World's Aircraft
- Manufacturer websites
- FAA AC 36-H1
- FAA/EASA Aircraft Type Certification Data Sheet
- NASA Technical Reports

Once the data is gathered, detailed models for the engine, airframe, and resulting noise are constructed. The resulting model is designed to meet published engine and vehicle performance data within one percent. As such these vehicles serve as important starting points for much of the analysis conducted using EDS. The current research focuses on applying the EDS baseline models to predict sources noise from en route aircraft.

2.0 Technical Progress

2.1 Description of EDS Automation

EDS was originally designed with a focus on the needs of CAEP. This meant that, from a noise perspective, EDS was set up to predict noise at the three standard noise certification points. Also, for fleet level analysis, EDS was setup to create NPD's in the terminal area, generally under 10,000 feet. Obviously the current focus on en route noise requires modification to allow EDS to generate source noise at high altitude. This requires converting the EDS setup of NASA's ANOPP, and modifying the EDS architecture to automatically generate source noise for en route over flights.

ANOPP uses two data tables, provided by the user, to describe the trajectory and engine operating conditions experienced by the aircraft. It then uses this information to predict the noise sources selected by the user. The first table to be changed was the FLIPATH table. Its components are the time, aircraft x position, aircraft y position, the 3 Earth fixed body Euler angles (ϕ_B, θ_B, and ψ_B), and the second body wind Euler angles (θ_{wb}, and ψ_{wb}). The values for aircraft y position, ϕ_B, ψ_B, θ_{wb}, and ψ_{wb} were fixed at zero for every segment of the en route conditions. Traditionally, EDS's vehicle analysis program, FLOPS, automatically generates this information for takeoff and landing trajectories; however, FLOPS does not have the built-in capability to generate this data for cruise. Therefore, algorithms were constructed within EDS to automatically parse the correct data from detailed mission summaries output by FLOPS. Since the goal is only to predict source noise and not propagation, time was given an arbitrary starting point and went in 10 second increments until all appropriate en route segments were covered. In other words, the time value serves as an index in this analysis. The appropriate en

route segments are top of climb, all cruise segments at their corresponding altitudes, and top of descent. It is worth noting EDS flies an aircraft using a "step-cruise." This is more representative of how aircraft are actually flown. The value for θ$_B$ was found by the following equation:

$$\theta_B = \tan^{-1}\left(\frac{\Delta z}{\Delta x}\right)$$

The second table was the FLIXX table. FLIXX's components are time, flight Mach number, engine power setting, speed of sound, density, dynamic viscosity, gear indicator, flap deflection, and absolute humidity. The gear indicator was defaulted to up at all times because the different flight segments en route would not have the gear down. The flap deflection and absolute humidity were defaulted to zero. Flight Mach number and the power setting were obtained by parsing the value from the FLOPS file for the corresponding altitude position that was given in the FLIPATH table. Speed of sound (ft/s), density (slug/ft^3), and dynamic viscosity (slug / ft-s) were obtained by using the following equations, given the altitude (z) of the aircraft.

If $z < 36089\,ft$

$$a = \sqrt{(1.4)(1716)(518.69)\left(1 - 6.875 \cdot 10^{-6}(z)\right)}$$

$$\rho = \left(1 - 6.875 \cdot 10^{-6}\right)^{4.2561}(.23769 \cdot 10^{-2})$$

$$\mu = .37373 \cdot 10^{-6}\frac{(518.69 + 216)}{(518.69(1 - 6.875 \cdot 10^{-6}(z)) + 216)}\left(\frac{518.69(1 - 6.875 \cdot 10^{-6}(z))}{518.69}\right)^{1.5}$$

If $z \geq 36089\,ft$

$$a = \sqrt{(1.4)(1716)389.97}$$

$$\rho = \left(1 - 6.875 \cdot 10^{-6}e^{(-(z-36089)/20806.7)}(.23769 \cdot 10^{-2})\right)$$

$$\mu = .37373 \cdot 10^{-6}\frac{(518.69 + 216)}{(389.97 + 216)}\left(\frac{389.97}{518.69}\right)^{1.5}$$

where :

$\mu = $ dynamic viscosity (slug / ft - s)

$a = $ ambient speed of sound (ft/s)

$\rho = $ density (slug/ft^3)

$z = $ altitude (ft)

To obtain values for all the different flight segments, the logic used to produce results for the FLIXX and FLIPATH tables explained above was implemented within a 'for' loop. This for loop took three data points from each of the different cruise, climb, and descent segments, and it concatenated them into a single file that would correspond to the en route FLIXX and FLIPATH tables. These tables would then replace any that were made for takeoff and landing by changing the logic in ANOPP to make it concatenate the en route text files instead of the others. Another change that was made to the logic of EDS was to make the state tables give

results for different Mach number and altitude combinations than those for takeoff and landing. The state tables within ANOPP contain corrected engine parameters such as mass flow, pressure, temperature, and rotational speed, as a function of ambient total temperature (or Mach number) and power setting. The altitude values were changed to altitudes that corresponded to the cruise and climb segments of each of the different passenger classes, and the Mach number values were changed to a range of values that would normally be encountered during the different aircrafts' operations en route. Because the project is mainly concerned with the noise produced by the engine, the portions of the ANOPP file that dealt with airframe noise were removed, allowing any results obtained to be purely for the engine noise. Furthermore, since the engine nozzle operating conditions are quite different between cruise and takeoff, it was decided to investigate whether or not shock cell noise needed to be included in the prediction of en route noise. In the traditional EDS setup, the shock cell noise prediction module in ANOPP was turned off under recommendation from the IRG. This makes sense since commercial engine nozzles are generally un-choked at takeoff and operate squarely in the subsonic regime.

2.2 Shock Cell Noise Investigation

Shock cell noise is generated when the nozzle of a turbofan is operating at relatively supersonic exhaust velocities and is not perfectly expanded. Under these conditions, shocks or expansions (depending on whether the nozzle is over-expanded or under-expanded) are formed at the nozzle exit and extend outward as defined by the relationship between the nozzle flow and the ambient. The intersection of a shock or expansion with the shear layer between the jet flow and the free stream ambient flow around the engine creates a reflection. As shown in Figure 1, the reflected shock or expansion will eventually intersect the opposite edge of the potential core, and another reflection will occur. This process forms a "shock cell" structure inside the potential core.
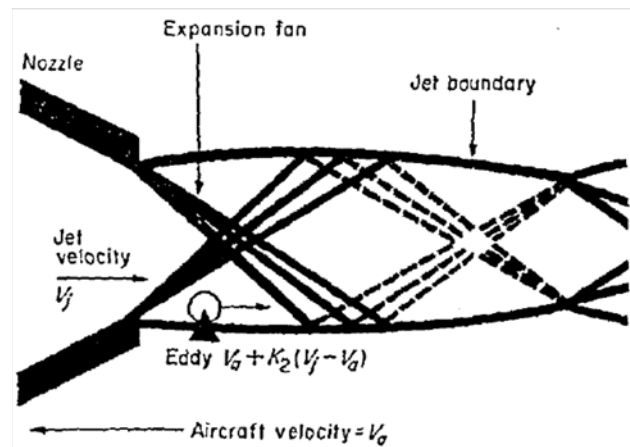
Figure 1: Shock Cell Noise Structure [11]

The noise is generated at each reflection because whenever the wave (shock/expansion) intersects with a region of different pressure, it causes a rapid change in pressure similar in nature to a small explosion. The noise is loudest forward of the engine, though the even spacing

of the series of shocks can generate coherent addition at various frequencies and angles. The level of the shock cell noise is a function of the difference between the actual nozzle Mach number and the design Mach number. A nozzle operating exactly at its design condition will produce no shock noise since no shocks will be created, but operating at either higher or lower speeds than the design condition will generate noise proportional to the velocity delta from the design Mach number. Shock cell noise is commonly accepted to be the loudest low frequency noise source during high altitude operations [10], especially at forward angles. Jet mixing noise is still significant, especially at more aft angles.
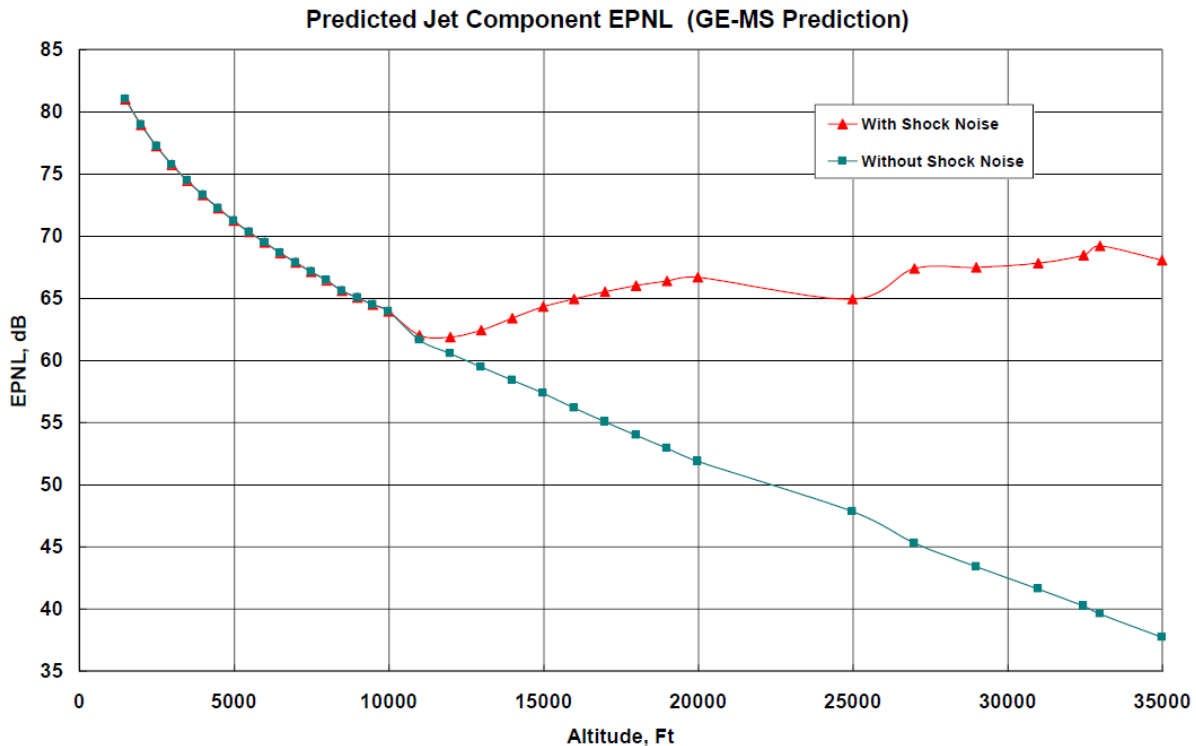
Figure 2: Magnitude of Shock Cell Noise at High Altitude [9]

A typical commercial turbofan engine does not have supersonic exhaust velocities at takeoff conditions in the vicinity of the airport, and never has supersonic exhaust velocities with the engines close to idle during approach. One result is that shock cell noise should not be present in any of the NPD's currently included in AEDT's ANP database. Thus, even though large distances are included in the NPD's, the noise levels are not appropriate for the prediction of en route noise. More generally, the relationship between aircraft noise levels near an airport may not scale to, or have any similarity to, cruise noise levels. Furthermore studies by Gliebe, reproduced in Figure 2, reaffirm that shock cell noise becomes the dominant noise source at cruise. [9] While the study by Gliebe confirmed the need to model shock cell noise at cruise and predicted the magnitude of such shocks, it serves a different purpose than the current research being conducted. The Gliebe study is very specific to a particular engine configuration and would be tedious to replicate for every engine within the AEDT database. It is more than likely

that the noise and engine performance codes used to generate the results in Figure 2 are at a similar, or higher, fidelity than EDS (described in section 2.1). This means there are hundreds of inputs that must be defined for a specific engine and airframe in order to generate meaningful results. Since a long term goal of the current research is a method that could be used within AEDT, the problem must be more constrained. A method must be formulated that requires as few as the five or so engine inputs represented in the AEDT database. As such, Gliebe's data substantiates the need for a method to predict en route noise for the fleet, but does not provide a solution. The primary goal of this research is to provide the solution, namely, a method to integrate into AEDT to predict shock cell noise en route.

Noise predictions in EDS are performed by ANOPP, a semi-empirical code comprised of modules for each noise source on a typical commercial aircraft. The data on which the acoustic predictions are based has been obtained over approximately the last twenty years; therefore, the predictions are calibrated to the technology present in the systems tested. Given the slow turnover rate of the commercial aircraft fleet, this technology assumption is quite appropriate for predictions involving the current fleet, as is the case for this research.

However, ANOPP was developed to predict community noise levels for takeoff and landing operations in the vicinity of airports. These are naturally low-speed, low-altitude operations, and the data obtained to support these predictions was generated under similar low-speed, low-altitude conditions. En route operations are high-speed and high-altitude, requiring a two-dimensional extrapolation of the underlying data in ANOPP. In addition, ANOPP has rarely been used at such conditions, making it possible to encounter limitations of the code imposed by programming decisions, rather than physics. Therefore, the primary goal of this research was to provide the solution, namely, a method to integrate into AEDT to predict shock cell noise en route.

2.3 Approach

As discussed previously, shock cell noise is a significant contributor to noise at altitude, but does not contribute significantly to terminal area noise. This makes it difficult to use NPD information from AEDT to predict en route noise since it will inherently lack any information about shock noise, either implicitly or explicitly. The AEDT database also lacks any detailed information about engine operating conditions, specifically the nozzle pressure ratios and geometries, needed to predict shock cell noise. Therefore, a new approach to predict en route noise is being proposed. Rather than using EDS to predict en route noise, a lower order engine sizing and performance prediction code was developed to estimate the nozzle conditions at cruise and climb segments. The lower order code was developed due to the following reasons:

- Implementing EDS into AEDT is not viable.
- Predicting the nozzle operating condition of an engine is a relatively a straightforward process that does not require a high fidelity engine performance code.
- The shock cell prediction algorithms do not need to run within ANOPP. This greatly reduces the data requirements and enables the use of a lower fidelity code.

MATLAB was used to create this low order code. The code was tuned using EDS as the "truth model" The low order model takes in known cycle information combined with tuning parameters, e.g. component efficiencies. It should be noted that the low-order engine performance model *is only suitable for use in predicting nozzle operating conditions for the purposes of estimating shock cell noise en route.* It should not be viewed as a general engine performance code. A flow path of the lower order engine/noise code is shown in Figure 3.
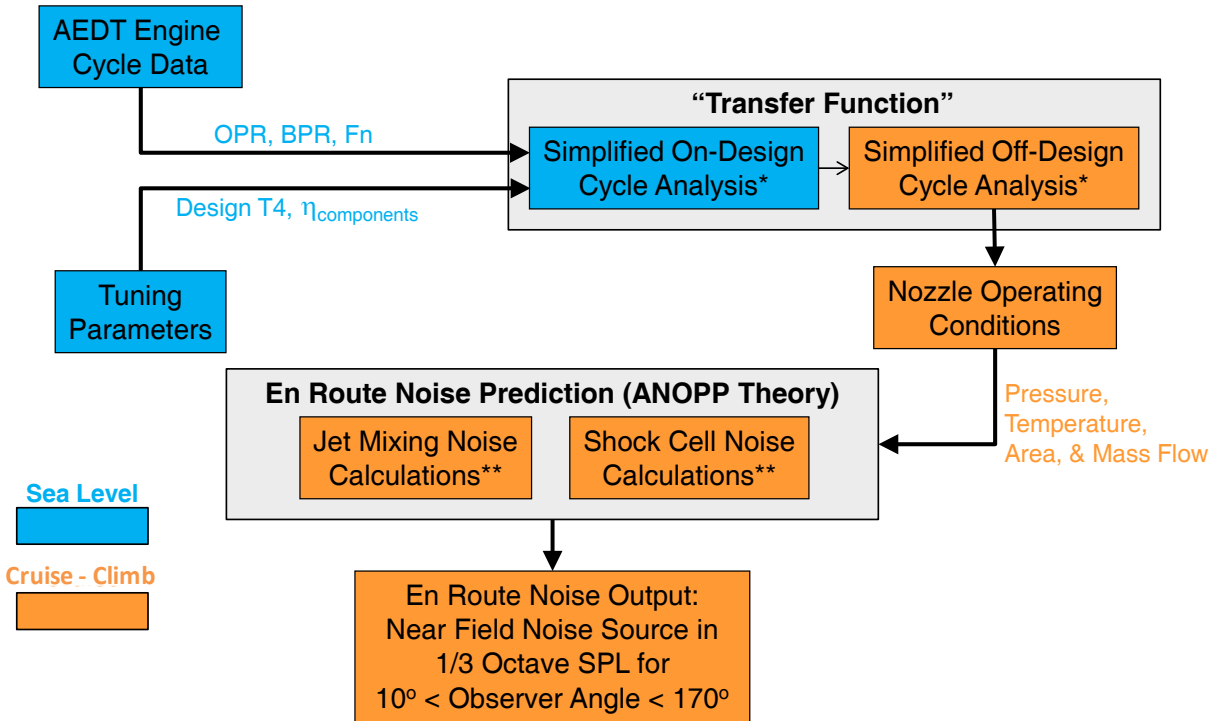
Figure 3: Low Order Engine and Noise Code Flow Path

2.4 Low-order Engine Code Creation

The first step in the routine was to create an on design algorithm, *"Simplified On-Design Cycle Analysis"*. The on design code specifies various engine design parameters and sizes the engine at a fixed point operating condition. That condition was defined as the maximum power at sea level static (SLS) conditions. SLS was chosen since it is the condition corresponding to the parameters provided in the AEDT/ICAO database. Design parameters consist of both specified parameters (OPR, BPR, Thrust), tuning parameters (component efficiency, design combustor temperature), and unknown parameters (FPR). During the on design process thrust is used to set the physical engine size, which remains fixed throughout the engine performance analysis.

The second step was to create an off design algorithm, *"Simplified Off-Design Cycle Analysis."* The off design code takes the fixed engine that was created in the on design code and "flies" it at different flight conditions to see how the engine performs. In a high fidelity engine simulation the component efficiencies change as a result of the assumed performance maps. For this code, efficiencies are assumed constant throughout the flight envelope. The off design code was coupled to the on design code and data passage between both codes was automated.

The resulting output data, specifically nozzle performance, *"Nozzle Operating Conditions"* from the off design conditions will be used to generate the noise of the engines at those given conditions. Details of the overall engine sizing and performance prediction code algorithm can be found in Appendix A. Low Order Engine Code Algorithm.

2.5 Code Calibration

The engine code was calibrated against different engines using available data from EDS. An overview of the calibration process is shown in Figure 4.
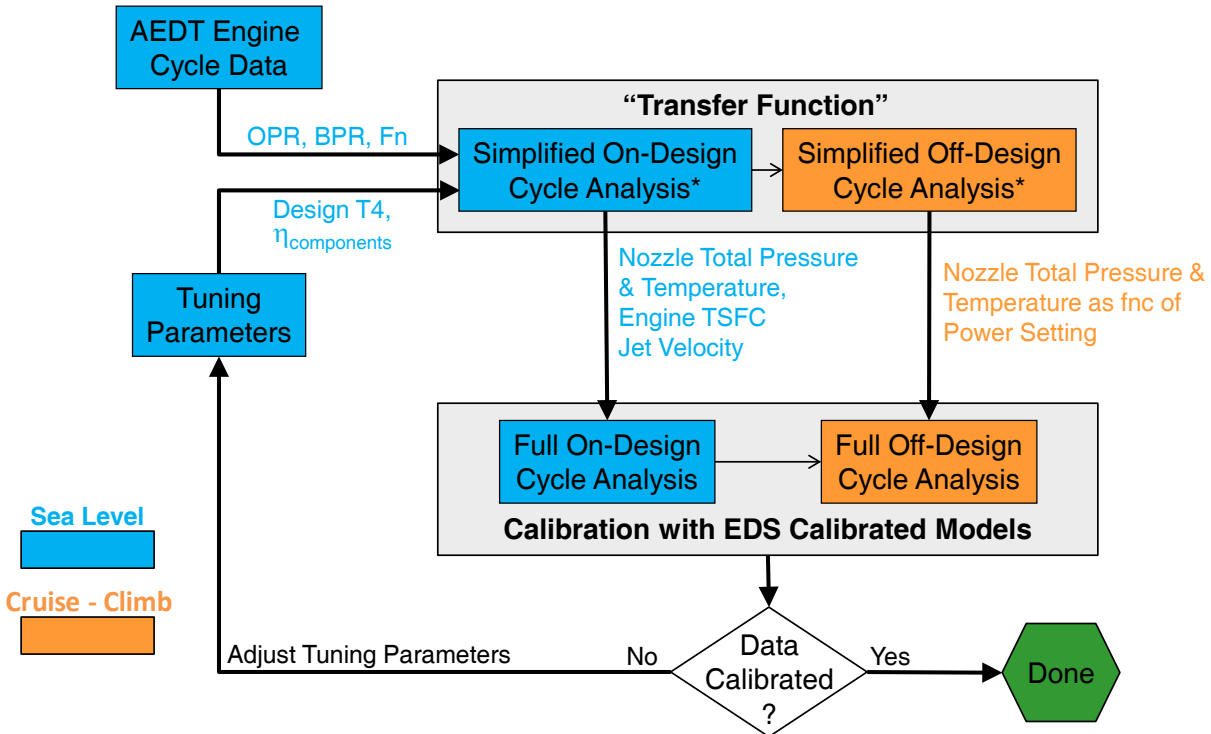
Figure 4: Low Order Engine Code Calibration Process

The OPR, BPR, T_{t4}, and Thrust at on design were set to the values used in EDS to mimic calibrated engines for the different passenger classes. To calibrate the code, a set of tuning parameters were used. The tuning parameters and their ranges are shown in Table 2.

To find the combination of tuning parameters would give the best result, the error of the code compared to EDS was recorded. The error was calculated by using a root mean squared error definition as shown below.

$$Error = \sqrt{\frac{(Code\ value_1 - EDS\ value_1)^2}{EDS\ value_1{}^2} + \frac{(Code\ value_2 - EDS\ value_2)^2}{EDS\ value_2{}^2} + \frac{(Code\ value_3 - EDS\ value_3)^2}{EDS\ value_3{}^2} + \cdots.}$$

(1)

Table 2: Tuning Parameters and Their Ranges

Input Parameter	Description	Min val.	Max val.
ξc	Adiabatic compressor efficiency	0.8	0.9
ξ_t	Adiabatic turbine efficiency	0.8	0.99
ξ_f	Adiabatic fan efficiency	0.85	0.99
$\xi_{mechanical}$	Mechanical efficiency	0.8	1.0
π_{nozzle}	Pressure ratio of the core nozzle	0.95	1.0
π_{fan}	Pressure ratio of the fan nozzle	0.95	1.0
π_d	Pressure ratio of the diffuser	0.97	1.0
γ_t	Specific heat of the turbine	1.3	1.35
c_{pc}	Specific heat of the compressor	0.216	0.264
c_{pt}	Specific heat of the turbine in	0.25	0.295
c_f	Cooling factor of bleed flows	1.0	1.35

The 'Code values' correspond to the values of each output variable of the code and the 'EDS values' are the corresponding values found when running EDS. For the purposes of calibration, the following parameters were tracked as responses to be matched against EDS provided outputs:

- SLS Nozzle Total Pressure
- SLS Nozzle Total Temperature
- High altitude nozzle total pressure with varying power setting
- High altitude nozzle total temperature with varying power setting
- Engine TSFC
- Jet Velocity

While the main engine cycle parameters were directly set by matching the engine cycle data from the EDS baseline model, a Latin Hypercube Design of Experiments (DoE) was constructed for the tuning parameters given in Table 2. Table 3 shows the final calibration factors for the different passenger classes when the error was minimized relative to the metrics listed above.

Since en route noise is the primary metric of interest, it was of importance to select final tuning parameters that not only minimized the rms error, but also captured appropriate trends in nozzle performance, including slope. The calibration charts for the five aircraft classes are shown in the appendix. Overall there is very good agreement considering that the EDS model capture significantly more real world effects and uses a more precise and detailed engine modeling code, the Numerical Propulsion System Simulation (NPSS).

Table 3: Tuning Parameters Values

Tuning Parameter	50PAX	150PAX	210PAX	300PAX	400PAX
ξ_c	0.875828	0.874268	0.887168	0.865702	0.857112
ξ_t	0.914442	0.853999	0.861662	0.96585	0.874925
ξ_f	0.975734	0.94849	0.941191	0.917167	0.954221
$\xi_{mechanical}$	0.843647	0.859367	0.837953	0.85626	0.972953
π_{nozzle}	0.964112	0.997968	0.958595	0.960312	0.974895
π_{fan}	0.955565	0.987232	0.976958	0.960048	0.950968
π_d	0.991393	0.982995	0.995139	0.981833	0.971651
γ_t	1.309828	1.308905	1.305138	1.315555	1.313705
c_{pc}	0.220382	0.240027	0.216699	0.22571	0.234885
c_{pt}	0.250615	0.281649	0.250046	0.274229	0.250361
c_f	1.11229	1.11951	1.10333	1.09527	1.07483

2.6 FPR Calculation

The value of FPR is generally unknown. An iteration loop around the on design code was required to calculate FPR. The loop starts with an initial assumption of FPR. The on design calculations are then performed. Both the core and bypass mass flows are outputs of the on design code. Using both, engine fan diameter can be calculated using the following equation:

$$D = 24 * \sqrt{\frac{\dot{m}_{core} + \dot{m}_{bypass}}{sizecoeff * 3.14 * (1 - \frac{1}{9})}} \tag{2}$$

This value is compared to the true fan diameter which is typically available in the literature. If the values are not equal, a new FPR value is picked and the on design calculations are repeated. The process continues until the chosen FPR value produces the correct fan diameter. To select the FPR value of the next iteration, the bisection method was implemented. A lower limit of 1 and an upper limit of 2 were used for FPR.

FPR calculation is also influenced by the 'sizecoeff' parameter in equation 2 which acted as an additional tuning parameter. Its value is engine dependent and a trial and error procedure was followed to determine its optimum value for each engine (the value that produced the least total rms error). Finally, since the FPR loop uses on design parameters, it is worth noting that the value of T_{t4} affects the on design calculations. T_{t4} values, as mentioned earlier, were fixed and were assumed based on the data of the calibrated engines in EDS. Table 4 shows a summary of the sizecoeff and T_{t4} values used for FPR calculation for the different vehicles.

Table 4: Values of 'sizecoeff' and 'T$_{t4}$'

Parameter	50PAX	150PAX	210PAX	300PAX	400PAX
sizecoeff	42.5	42.5	42.5	42.5	39.5
T_{t4}	2868.64	3038.57	3167.33	3210.21	2810.85

3.0   En Route Noise Prediction Method

Following the results of the studies Gliebe, it was proposed that the noise model for both climb and cruise may comprise only jet noise because of its dominance over other sources. To validate this assumption, the engine noise was modeled using ANOPP with and without shock cell noise to assess the error at varying altitudes and operating parameters. The results agreed with the Gliebe study, and are detailed in section 3.1. A noise model was developed based on ANOPP's Stone Jet Noise Module, and is described in section 3.2.

Because of greatly reduced engine throttle during descent, the engine noise was thought to be dominated by airframe noise during this segment. A study was performed to confirm this assumption as detailed in section 3.3. A second model was then developed based on the Fink Airframe Noise Module (FNKAFM, [10]) to predict noise during descent, and is detailed in section 3.4.

3.1 Jet Noise Dominance Validation

In order to validate the assumption that jet noise was dominant during climb and cruise, two studies were performed. For each study, EDS was used to model the aircraft from each passenger class to gather climb and cruise trajectory data from FLOPS at altitude, performance data from NPSS at altitude, and other aircraft specific parameters. This data was used to construct an ANOPP model reflecting the appropriate conditions during the climb and cruise segments above 15,000 ft.

The trajectory data reported by FLOPS is output in a table form with operating conditions for a series of points in the profile. Points were selected from the table in the altitude range of 15,000 to 25,000 ft for the climb segment with approximately even altitude spacing, and one point was selected at the beginning of the cruise segment. NPSS was then used to generate performance data for each of these profile points for use in the ANOPP model. Instead of using the FLOPS generated trajectory, steady flyover trajectories were generated for the conditions at each profile point. Because the observer is fixed in the ANOPP model, this removed any bias for directivity variation throughout the true trajectory. This method essentially models the source exactly as it produced at the profile point and moves it through a steady flyover above the observer. Because only the relative source levels are required (jet vs. fan vs. airframe etc.), the variation in speed at each point was not an issue.

At this point, the two studies diverged. In the first study, an observer was placed 4 ft above the ground, and the ANOPP propagation model was used to model the received noise. While this propagation model is not accurate for high altitude, it provides a general idea of magnitude of the frequency dependent atmospheric attenuation. For each case, the jet noise

was compared to the noise from all components including the other engine components and the airframe components as seen in Figure 5.
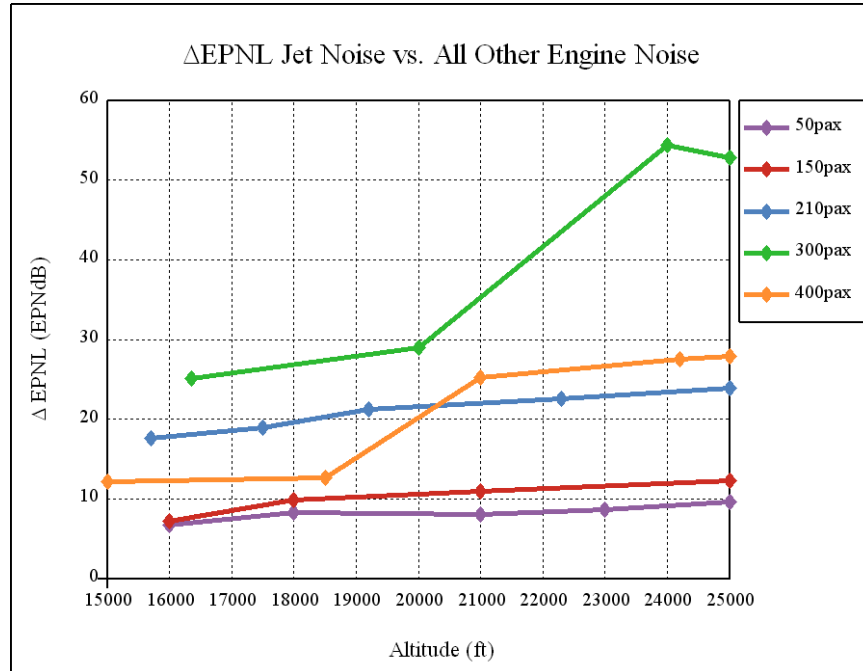
Figure 5: EPNL Difference of Total Jet Noise vs. All Other Engine Components

A common rule of thumb in acoustics states that for two sources with a difference in level of 10dB, the quieter source cannot be heard due to masking by the louder source. The difference in EPNL between jet-only versus all other sources at each altitude above 18,000 ft. was greater than 10EPNdB for all vehicles except the 50pax model supporting the assumption that jet noise is dominant at altitude for these vehicles. It should be noted that the 10dB rule was set for comparison of SPL values. The EPNL metric modifies and averages the SPL spectra of an operation applying weighting for frequency, tones, and duration that are perceived as louder or more annoying by humans. Thus, a delta of EPNdB is not directly comparable to a delta of dB SPL. Due to the modifications for human perception, a change in EPNdB, the 10dB rule may be relaxed a bit for this metric. It was therefore assumed that the difference in EPNdB between the jet vs. all other engine components for the 50pax model, though less than 10dB, was still sufficiently great to ignore all engine components accept the jet in the noise prediction. In addition, an examination of the error in EPNL was performed to quantify the error in the EPNL predicted when only the jet was modeled vs. the total aircraft. Because of the relative dominance of the jet, the maximum EPNL error was less than 0.9 EPNdB for all passenger class models at each altitude Figure 6. This further supported the jet only assumption.
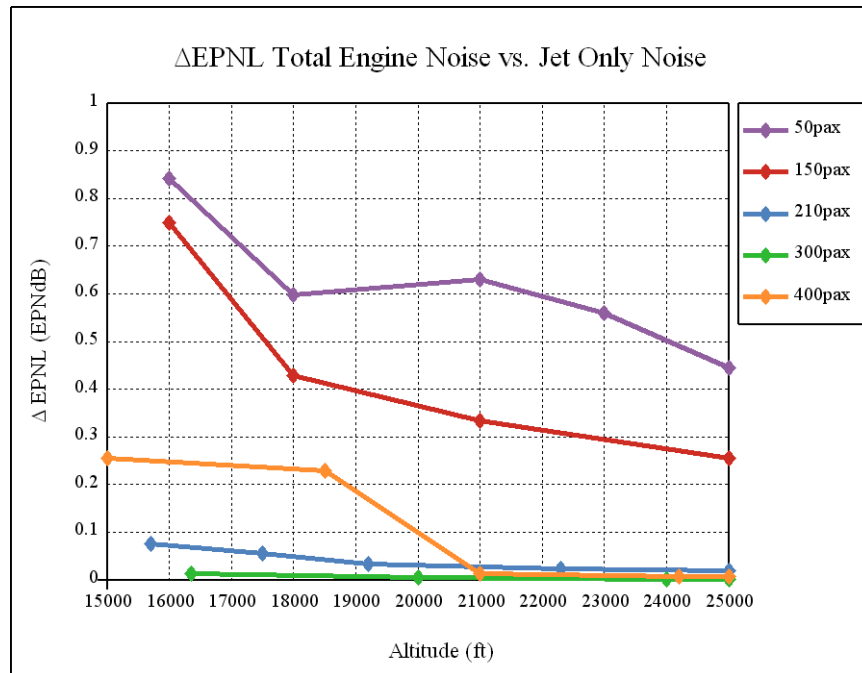
Figure 6: EPNL Calculation Error with Jet Only (Total EPNL Minus Jet EPNL)

In the second study, the instantaneous sound levels at an observer distance of 1 ft. were compared for the jet vs. all other components. This eliminates any bias error inherent in the propagation model. Still, the general frequency dependence of the atmospheric attenuation must be considered when reviewing the results. First, the directivity dependent spectra were summed to an OASPL as a function of directivity angle, and the values for both source groups were compared at each altitude. Figure 7 shows the results of this study for the 150pax model, and results for the other models may be found in the appendix. It is clear that the OASPL of the jet was greater by at least 2 dB OASPL for each observer angle at each altitude. In fact, for the majority of the directivity angles at each altitude, the OASPL of the jet source was much greater than that of the rest of the sources. Because the aircraft angle of attack is increased during climb, the noise generated for an observer angle less than 30° will likely have little to no effect on the noise level on the ground. This eliminates several values at which the jet noise dominated to a lesser degree. By the same token, the noise emitted at aft observer angles will likely have a greater effect on the ground level noise. This accentuates the values at which the jet was most dominant.

ANOPP provides as output tables of noise spectra for each source as a function of the directivity angle. The SPL tables for all sources excluding the jet were summed, and the SPL of these combined sources was compared to the jet SPL for each value in the tables. The results for the 150pax model at 19000 ft can be seen in Figure 8. All values in which the jet noise level was less than the rest of the combined sources occurred at frequencies above 1000 Hz. We can ignore these values, keeping in mind that noise at these frequencies will be most affected by atmospheric attenuation.

Figure 7: 150pax ∆OASPL Jet Noise vs. All Other Engine Noise
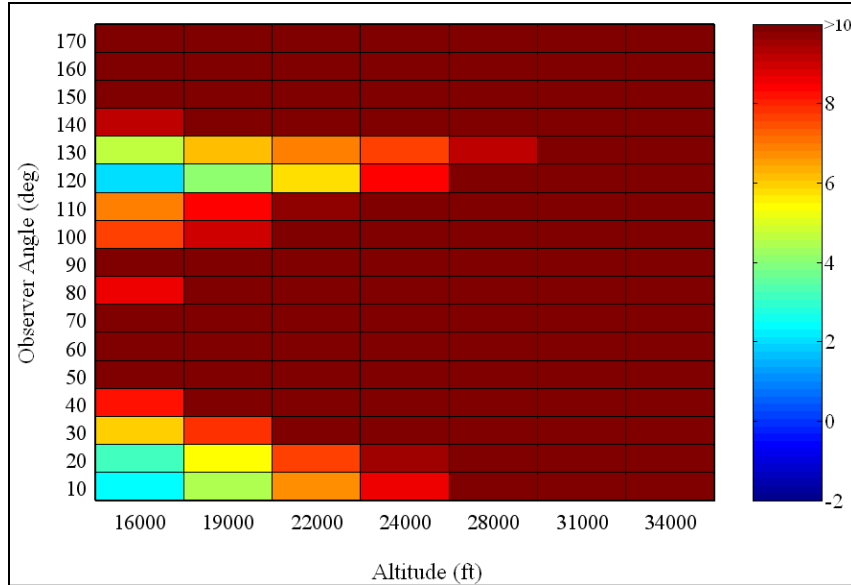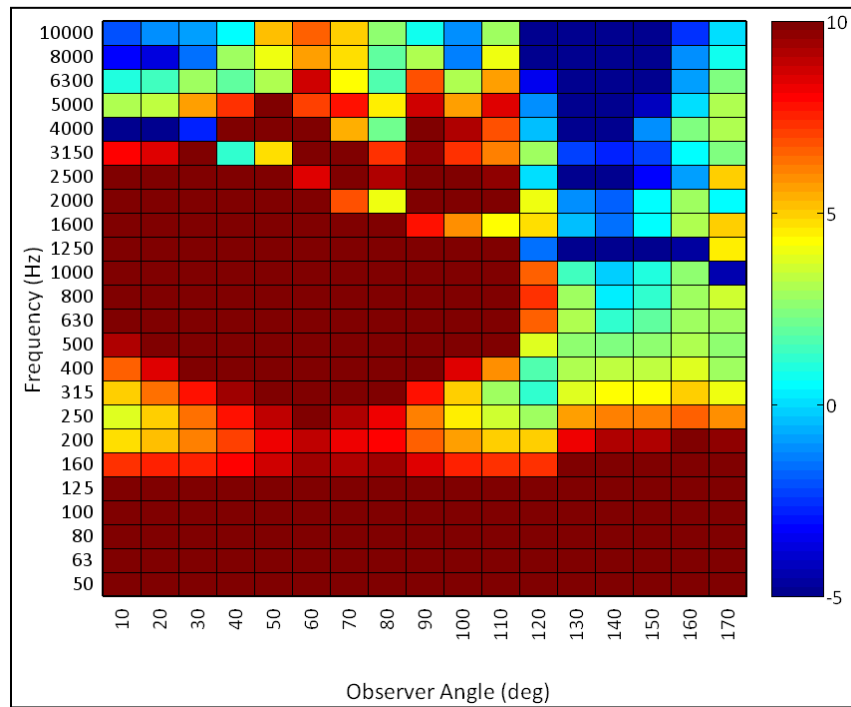

Figure 8: 150pax ∆SPL Jet Noise vs. All Other Engine Noise for 19,000 ft

3.2 Climb and Cruise Noise Prediction Method

3.2.1 Method

A noise prediction method based on the ST2JET module within the ANOPP framework has been developed. The ST2JET methodology was developed from data with bypass ratios

ranging from 5.0 to 14.9 obtained within free jet facilities at freestream Mach numbers ranging from 0.0 to 0.28—both anechoic and non-anechoic. The freestream Mach number range for the developmental data set is a limitation of ST2JET methodology. However, because the published capability of ST2JET extends to a freestream Mach number of 0.9, the ST2JET methodology is very capable of predicting jet noise for the current in-service fleet of turbofan aircraft.

The en route noise prediction method developed during the current work predicts jet noise for circular exhaust nozzles having a single stream or two coannular streams, convergent geometry, and subcritical or supercritical pressure ratio at typical cruise velocities and altitudes. It accounts for the presence of center plugs where the tip radius of the plug is zero. It does not account the presence of non-zero-tip-radius center plugs or the presence of noise suppression devices. Jet noise from both conventional and inverted velocity profiles is predicted. The noise is predicted at a reference location one foot below the aircraft at observer angles ranging from 0° to 170° (measured from nose of the aircraft) for one-third octave bands ranging from 50 Hz to 10 kHz.

The equations and tabulated coefficients provide in the Reference [10] for the following jet noise components were coded into the new en route noise prediction MATLAB script. Those jet noise components not included in the current prediction method are outside of the scope of the present work.

- Intermediate Scale Inner Stream Mixing Noise
- Small Scale Outer Stream Mixing Noise
- Large Scale Merged Stream Mixing Noise
- Inner Stream Shock Noise
- Outer Stream Shock Noise
- Plug/Downstream Merged Shock Noise

The en route noise prediction script requires input of ambient flow conditions, nozzle flow properties, and geometric dimensions of the nozzle. Many of input parameters are provided by the low-order engine performance prediction code described above. Those inputs provided by the low-order engine performance prediction script for the en route noise prediction script are provided in the Table 5.

In addition to the input parameters included in Table 5, the outer diameters of the primary and secondary nozzle are required. Those values are not included in the AEDT database; however, AEDT uses passenger-class-specific values for these quantities when generating noise prediction inputs for ANOPP. Those class-specific values are used in the current en route noise prediction script and are tabulated in Table 6.

Any primary or secondary jet flow properties computed in the ST2JET method not given by the low-order engine performance prediction script are computed in the en route noise prediction script using the equations given in Reference [10]. These computed properties are:

- Jet Mach Numbers
- Jet Static Temperatures
- Sound Speeds within the Jets
- Jet Velocities
- Jet Densities

- Jet Molecular Weights
- Hydraulic Exit Diameters
- Hydraulic Throat Diameters
- Ideal Jet Flow Areas

Table 5: Input Parameters for Cruise/Climb En Route Noise Prediction Method

Input Parameter	Description	Units
M_∞	Ambient Mach Number	
P_∞	Ambient Static Pressure	lbf/ft^2
T_∞	Ambient Temperature	°R
c_∞	Ambient Speed of Sound	ft/sec
ρ_∞	Ambient Density	slugs/ft^3
T	Engine Net Thrust	lbf
A_1	Primary Jet Nozzle Area	ft^2
A_2	Secondary Jet Nozzle Area	ft^2
$\dot{m}_1$	Primary Jet Nozzle Mass Flow Rate	slugs/sec
$\dot{m}_2$	Secondary Jet Nozzle Mass Flow Rate	slugs/sec
$P_{t,1}^*$	Primary Jet Nozzle Total Pressure/Ambient Static Pressure	
$P_{t,2}^*$	Secondary Jet Nozzle Total Pressure/Ambient Static Pressure	
$T_{t,1}^*$	Primary Jet Nozzle Total Temperature/Ambient Static Temperature	
$T_{t,2}^*$	Secondary Jet Nozzle Total Temperature/Ambient Static Temperature	
γ_1	Primary Jet Ratio of Specific Heats	
γ_2	Secondary Jet Ratio of Specific Heats	
R_1	Primary Jet Gas Constant	ft-lbf/lbm/°R
R_2	Secondary Jet Gas Constant	ft-lbf/lbm/°R
$noEng$	Number of Engines	

Table 6: Passenger-Class-Specific Nozzle Outer Diameters

Passenger Class	Primary Nozzle Outer Diameter, $d_{1,o}$ (ft)	Secondary Nozzle Outer Diameter, $d_{2,o}$ (ft)
50	2.10	4.67
150	2.97	5.08
210	3.46	8.67
300	5.15	10.17
500	5.15	10.17

All merged jet flow properties computed in the ST2JET method are computed in the en route noise prediction script using the equations given in Reference [10].

3.2.2 Validation

The accuracy of the en route noise prediction MATLAB script was assessed using comparison with actual ANOPP ST2JET results. The engine input parameters for the noise prediction script were matched with the ANOPP input parameters given in the output file, thus enabling a one-to-one comparison of the results. The results from this comparison for the 150 passenger class aircraft equipped with the EDS baseline engine are shown in Figure 9. The difference in sound pressure level ($\Delta SPL = SPL_{SCRIPT} - SPL_{ANOPP\ ST2JET}$) is shown for power settings of 76% (a) and 100% (b). The results for the lower power setting differ by as much as 3.3 dB, while at the maximum power setting the difference reaches 1.9 dB at its peak. Since atmospheric absorption is dependent upon frequency to the extent that source noise (i.e., the noise that is predicted 1 foot from the aircraft) above 1 kHz will typically not be heard by a ground observer, results above 1 kHz can be ignored. Additionally, the differences for the frequency range of interest (i.e., 50 to 1000 Hz) shown in Figure 9 are negligible. Therefore, it can be concluded that the accuracy of the en route noise prediction MATLAB script is practically equivalent to that of the ANOPP ST2JET module. The results shown in Figure 9 are representative for those generated for all other aircraft passenger classes.

The discrepancy in the results for the different power settings (i.e., maximum difference of 3.3 dB for 76% power and 1.9 dB for 100% power) shown in Figure 9 can be explained by the physical logical within the ST2JET methodology which is consistent with that formulated in the MATLAB script. The spectra at both power settings are primarily dominated by the shock-associated broadband noise. In all instances, the shock-associated broadband noise is comprised of a combination of three shock noise components:

- Inner Stream Shock Noise
- Outer Stream Shock Noise
- Plug/Downstream Merged Shock Noise

The inner stream shock noise is computed only if the primary stream would be supersonic if it were to be fully expanded. The outer stream shock noise is computed only when both the primary and secondary streams are supersonic when fully expanded and the plug/downstream merged shock noise is not applicable. The plug/downstream merged shock noise is present only when both streams are fully-expanded supersonic and the total pressure in the secondary stream is greater than or equal to that in the primary stream.

For the 76% power case, the shock-associated broadband noise is computed as the inner and merged stream shock noise. For the maximum power case, the shock noise is due to inner and outer stream shock noise. Therefore, the discrepancy in the results for the different power settings is attributed to the shock noise components used to compute the results.
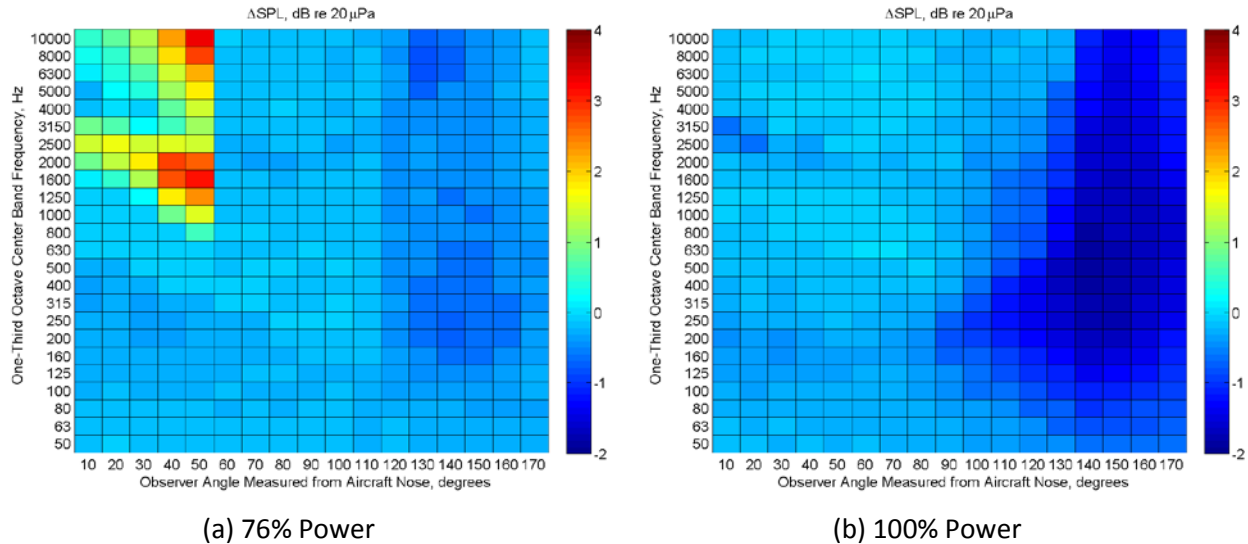
(a) 76% Power   (b) 100% Power

Figure 9: SPL Differences for 150pax Baseline Engine

3.3 Airframe Noise Dominance Validation

In order to validate the assumption that airframe noise was dominant during descent, two studies were performed. For each study, EDS was used to model the aircraft from each passenger class to gather descent trajectory data from FLOPS at altitude, performance data from NPSS at altitude, and other aircraft specific parameters. This data was used to construct an ANOPP model reflecting the appropriate conditions during the descent segment above 15,000 ft.

The trajectory data reported by FLOPS is output in a table form with operating conditions for a series of points in the profile. A selection of 5 points was made from the table in the altitude range of 15,000 to 25,000 ft with approximately even spacing. NPSS was then used to generate performance data for each of these profile points for use in the ANOPP model. Instead of using the FLOPS generated trajectory, steady flyover trajectories were generated for the conditions at each profile point. Because the observer is fixed in the ANOPP model, this removed any bias for directivity variation throughout the true trajectory. This method essentially models the source exactly as it produced at the profile point and moves it through a steady flyover above the observer. Because only the relative source levels are required (jet vs. fan vs. airframe etc.), the variation in speed at each point was not an issue.

At this point, the two studies diverged. In the first study, an observer was placed 4 ft above the ground, and the ANOPP propagation model was used to model the received noise. While this propagation model is not accurate for high altitude, it provides a general idea of magnitude of the frequency dependent atmospheric attenuation. For each case, the airframe noise was compared to the noise from all other components. The difference in EPNL for each vehicle at each altitude was greater than 10EPNdB supporting the assumption that airframe noise is dominant at altitude.

In the second study, the noise generated by each source at a distance of 1 ft. was compared. The directivity dependent spectra were summed to an OASPL as a function of

directivity angle, and these values were compared between each source for each altitude, eliminating any bias error inherent in the propagation model. At each directivity angle and each altitude, the airframe noise OASPL was 10 dB greater than all other aircraft noise components combined.

3.4 Descent Noise Prediction Method

3.4.1 Method

A noise prediction method based on the FNKAFM module within the ANOPP framework was developed. The FNKAFM methodology was developed using both physical formulas and empirical formulas generated with data from flyover noise measurements of several aircraft of varying sizes. The free stream Mach number range for the developmental data set is again a limitation of this methodology. However, here too the published limits of the method showed a range of 0.0 to 0.9, and was thus deemed fit for this effort.

Because the geometric configurations of the aircraft of interest, namely all those modeled within AEDT, is so diverse, a single dominant airframe source could not be identified. In addition, with a lower altitude bound of 15,000 ft, it was assumed that the landing gear would not be deployed. The prediction method thus does not include a calculation for landing gear noise. Additionally, it is assumed that no delta wings will be included, and that the wing is not clean. The method is able to perform all other functionality of the FNKAFM module with prediction all sources including wing trailing edge noise, horizontal tail trailing edge noise, vertical tail trailing edge noise, leading edge slat noise, and trailing edge flap noise, and excluding landing gear noise. The noise is predicted at a reference location one foot below the aircraft at observer angles ranging from 0° to 170° (measured from nose of the aircraft) for one-third octave bands ranging from 50 Hz to 10 kHz.

The en route noise prediction script requires input of ambient flow conditions and aircraft geometry. Many of input parameters are provided by the low-order engine performance prediction code described above. Those inputs provided by the low-order engine performance prediction script for the en route noise prediction script are provided in Table 7.

3.4.2 Validation

The method employed uses the exact formulation as the ANOPP model along with the same inputs. Thus, no error should be observed. However, some rounding error does manifest due to discrepancies in the allowable number of significant figures for each model. To quantify this error, a 10,000 case Latin Hyper Cube design of experiments – chosen for its space-filling capabilities – was generated for the full ranges of the input parameters. Both the FNKAFM module and the Matlab version were run, and the results were compared. The average absolute error was very small at 0.002dB, and the maximum absolute error of 0.4dB was within the round-off error limit. The distribution of this error was random throughout each angle/frequency combination.

Table 7: Input Parameters for Descent En Route Noise Prediction Method

Input Parameter	Description	Units
A_f	Total Flap Area	ft^2
A_h	Total Horizontal Tail Area	ft^2
A_v	Total Vertical Tail Area	ft^2
A_w	Total Wing Area	ft^2
B_f	Total Flap Span	ft
B_h	Total Horizontal Tail Span	ft
B_v	Total Vertical Tail Span	ft
B_w	Total Wing Span	ft
N_s	Number of Trailing Edge Flap Slots	
c_∞	Ambient Speed of Sound	ft/sec
M_∞	Ambient Mach Number	
ρ_∞	Ambient Density	slugs/ft^3
μ_∞	Ambient Dynamic Viscosity	slugs/ft^3

4.0   En Route Noise Prediction Results

4.1 Climb/Cruise Results

Results obtained using the en route noise prediction method developed during this work are presented below. The results shown below were produced using input parameters generated using the low-order engine performance script described above. The input parameters to the low-order engine performance script include flight altitude and engine parameters available in the AEDT database—engine overall pressure ratio, engine bypass ratio, and sea level static thrust.

All relative sound pressure levels (ΔSPL = SPL$_{SCRIPT}$ - SPL$_{ANOPP\ ST2JET}$) are shown at a reference location one foot below the aircraft at observer angles ranging from 0° to 170° (measured from nose of the aircraft) for one-third octave bands ranging from 50 Hz to 10 kHz. The results are presented as the difference between EDS/ANOPP and the low order code for all baseline engines for each of the passenger classes—50PAX (Figure 15), 150PAX (Figure 16), 210PAX (Figure 17), 300PAX (Figure 18), and 500PAX (Figure 19). Where available, results are shown for power settings of 100% and below.

With the new FPR determination method, the FPR was matched based on fan diameter calculations, and the results mirror the prediction with "known" FPR. Two sets of runs are presented, one for the case where the fan pressure ratio (FPR) is matched based on fan diameter, and one showing previous results where the low order engine performance code is allowed to choose the FPR that minimizes TSFC for a given BPR, OPR, and SLS thrust. In the comparisons where the FPR in the low order code is manually set to match the calibrated value from EDS, the code performs relatively well with the maximum errors at maximum power and cruise power in SPL as shown in Table 8 and Table 9 and Figure 10 through Figure 14.

Table 8: Low Order Noise Prediction Error Relative to EDS at 100% Power

PAX Class	Max SPL Error with FPR determined by fan diameter, FPR shown in parentheses	Max SPL Error with FPR Search, FPR shown in parentheses
50	1.1 dB (1.547)	36.6 dB (1.783)
150	5.9 dB (1.693)	20.5 dB (1.800)
210	5.6 dB (1.705)	19.3 dB (1.800)
300	2.7 dB (1.619)	18.4 dB (1.667)
500	1.5 dB (1.581)	21.9 dB (1.547)

Table 9: Low Order Noise Prediction Error Relative to EDS at Partial Power

PAX Class	Max SPL Error with FPR determined by fan diameter, FPR shown in parentheses	Max SPL Error with FPR Search, FPR shown in parentheses
50	1.9 dB (1.547)	37.1 dB (1.783)
150	4.1 dB (1.693)	4.1 dB (1.800)
210	4.1 dB (1.705)	5.2 dB (1.800)
300	6.7 dB (1.619)	6.4 dB (1.667)
500	1.9 dB (1.581)	22.2 dB (1.547)

Detailed errors between the EDS/ANOPP predictions and the manually set FPR noise predictions are shown in Figure 10 through Figure 14. Maximum absolute errors range from 1.1 dB to 6.7 dB. This variation in the relative results is much smaller than that when the 'optimum' FPR is determined using the minimum TSFC search routine.
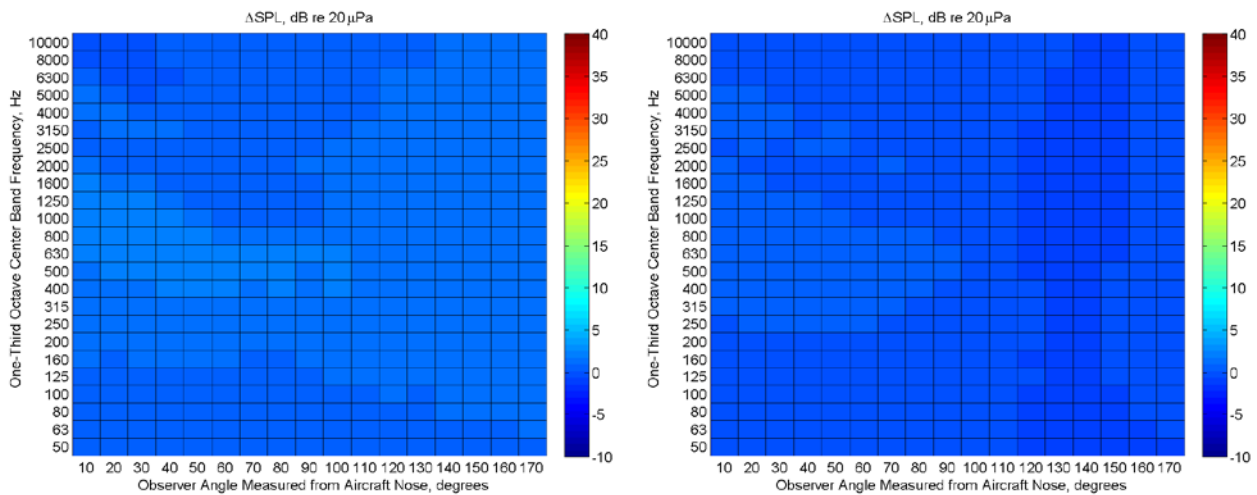
(a) 83% Power   (b) 100% Power

Figure 10: Relative Results for the 50pax Baseline Engine
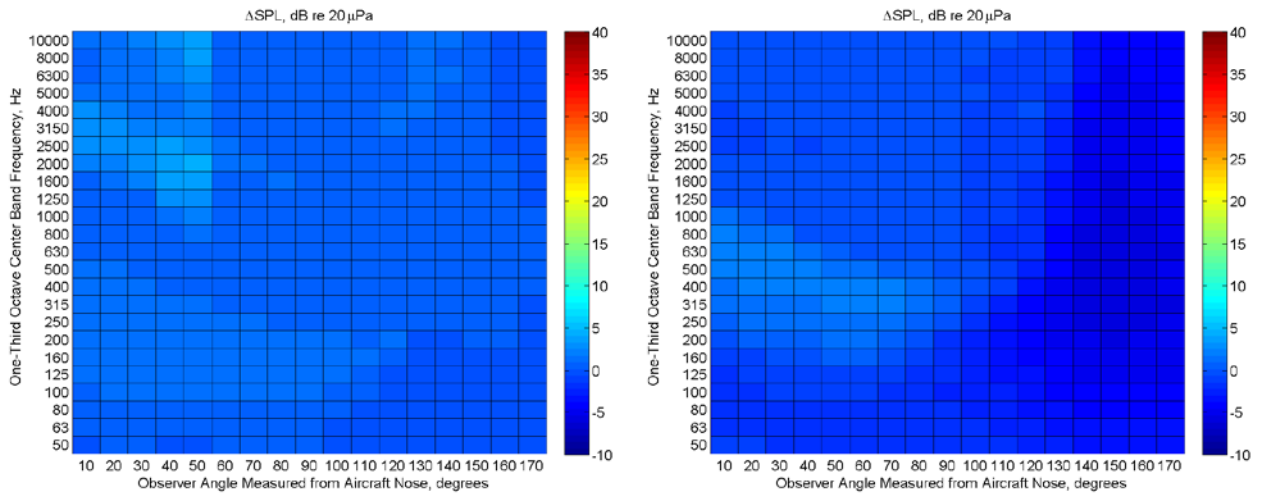
(a) 76% Power   (b) 100% Power

Figure 11: Relative Results for the 150pax Baseline Engine
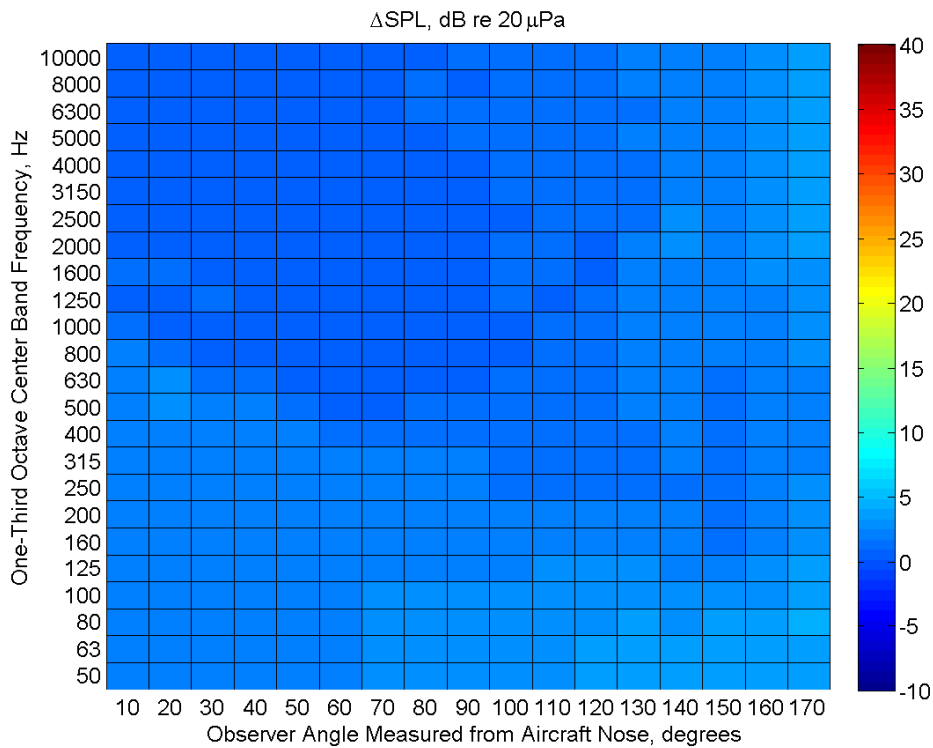
Figure 12: Relative Results for the 210pax Baseline Engine at 89% Power

(a) 82% Power   (b) 100% Power
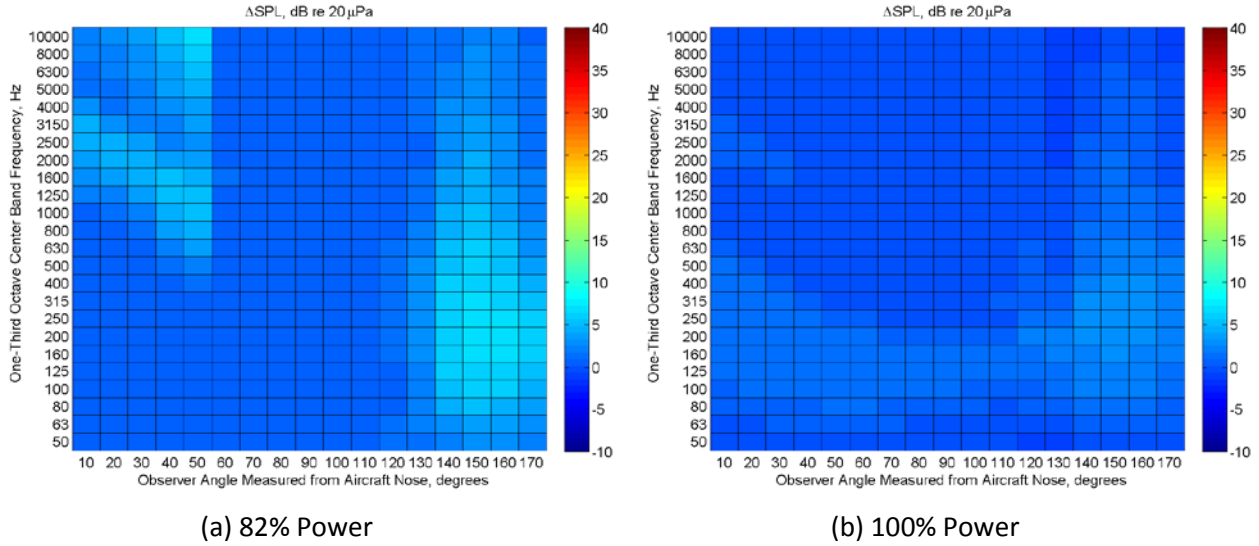
Figure 13: Relative Results for the 300pax Baseline Engine

(a) 93% Power   (b) 100% Power
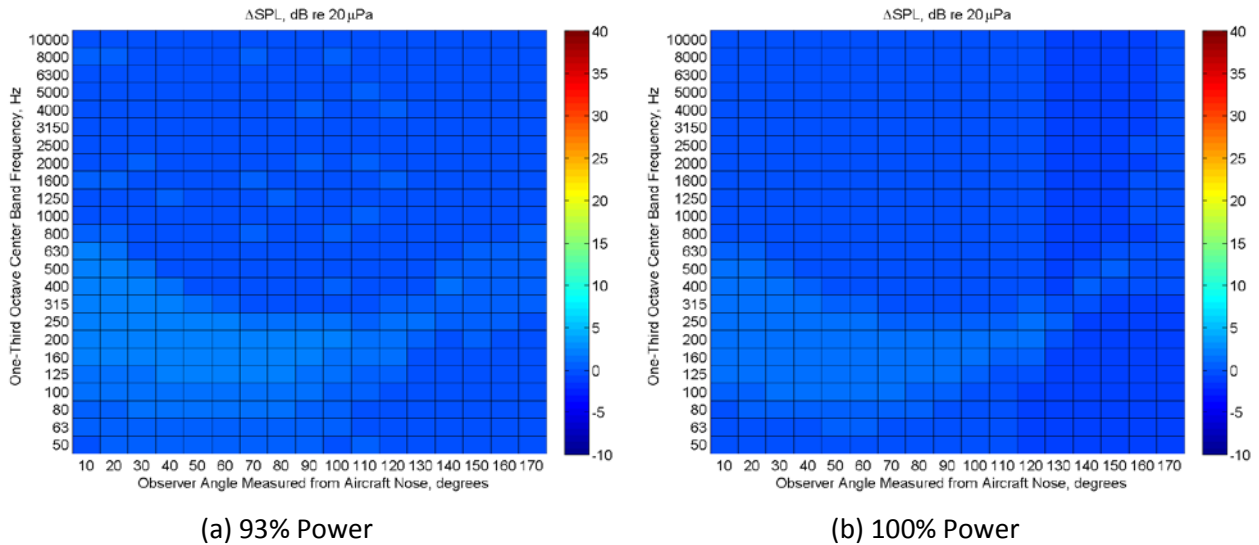
Figure 14: Relative Results for the 400pax Baseline Engine

However, when the code is allowed to search for the 'optimum' FPR, as in results from year 1, the results are inconsistent over the range of engine sizes and power settings. In reality, many other factors such as cost, engine diameter constraints, existing engine core design limitations, operability issues, and other items may prevent the designer from choosing the FPR that is the thermodynamic optimum. This is part of the reason the EDS FPR does not match the low order FPR when allowed to optimize for minimum TSFC. More detailed errors between the EDS/ANOPP predictions and the low order code are shown in Figure 15 through Figure 19. Over the ranges of passenger classes and power settings, the absolute maximum differences vary from 4.1 dB to 37.1 dB. This is an extremely large variation in the relative results. The noise prediction generated using the ST2JET methodology is highly dependent upon the engine parameter inputs, specifically primary and secondary stream total pressure. Small

discrepancies in actual and predicted total pressures tend to produced large differences in the noise results.

(a) 83% Power (b) 100% Power
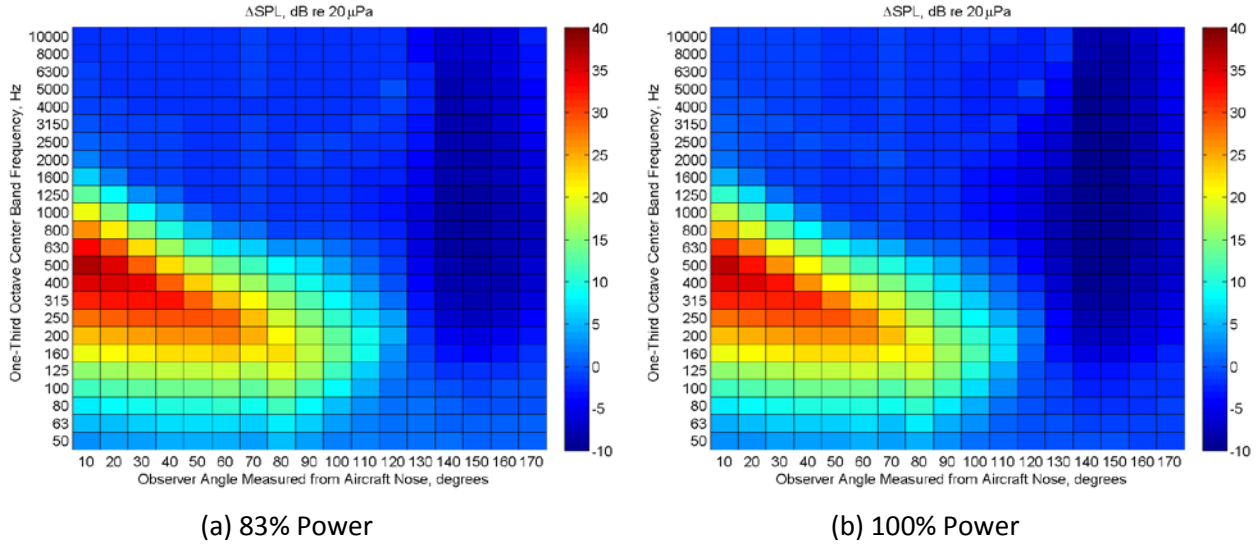
Figure 15: Relative Results for the 50pax Baseline Engine (FPR Search)

(a) 76% Power (b) 100% Power
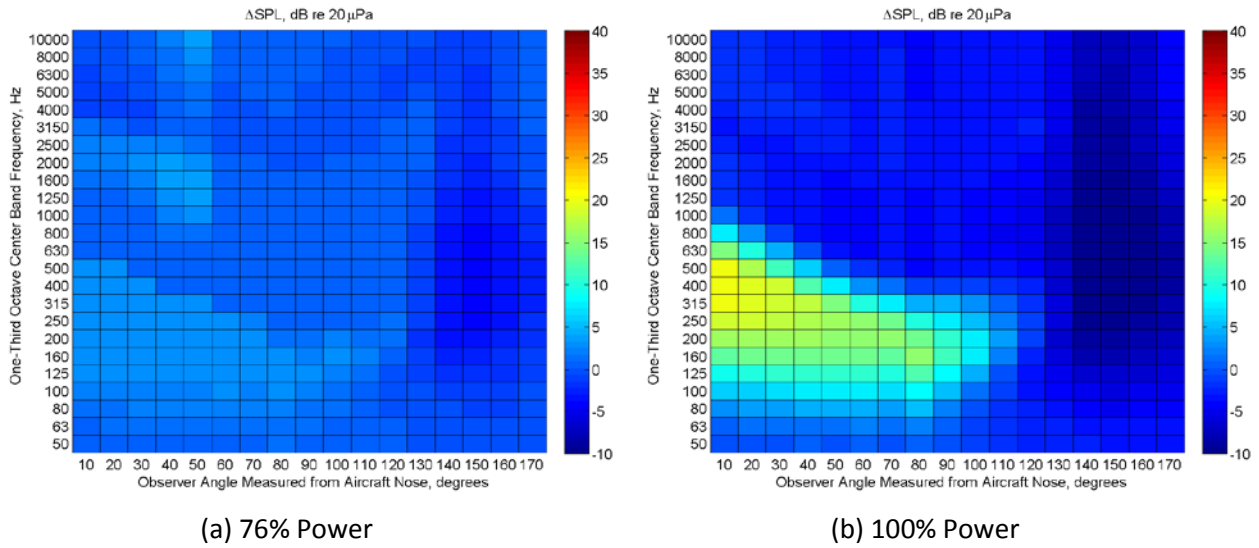
Figure 16: Relative Results for the 150pax Baseline Engine (FPR Search)

ΔSPL, dB re 20 μPa

One-Third Octave Center Band Frequency, Hz

Observer Angle Measured from Aircraft Nose, degrees

Figure 17: Relative Results for the 210pax Baseline Engine at 89% Power (FPR Search)
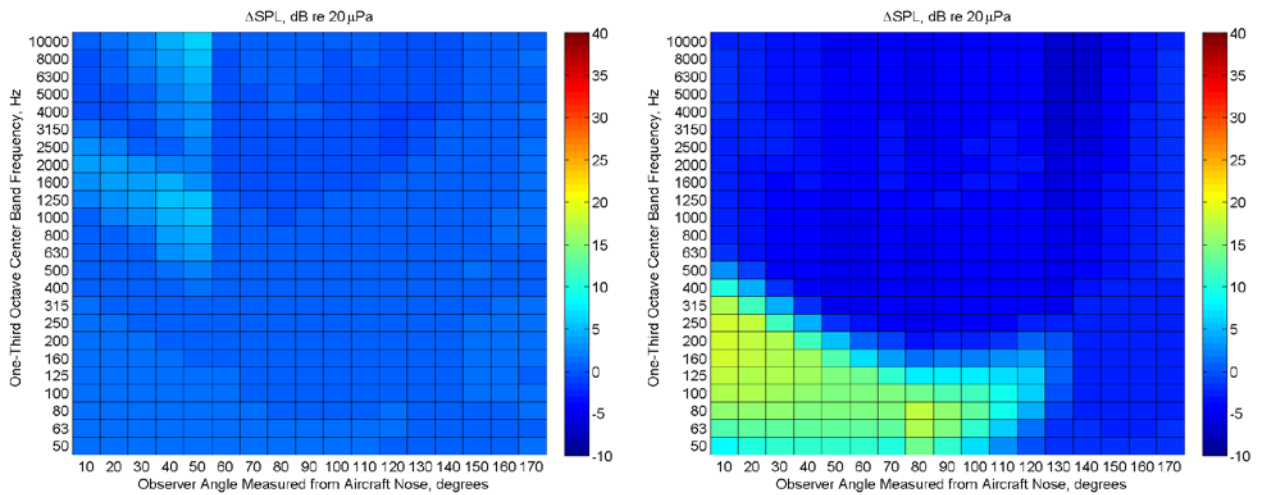
(a) 82% Power

(b) 100% Power

Figure 18: Relative Results for the 300pax Baseline Engine (FPR Search)

(a) 93% Power   (b) 100% Power
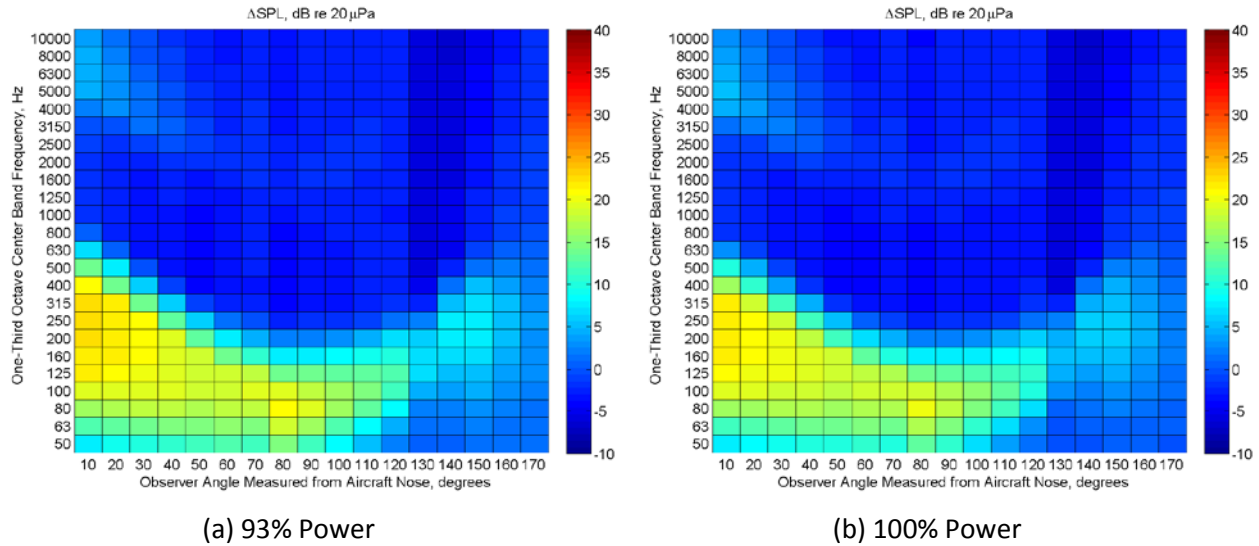
Figure 19: Relative Results for the 400pax Baseline Engine (FPR Search)

4.2 Approach Results

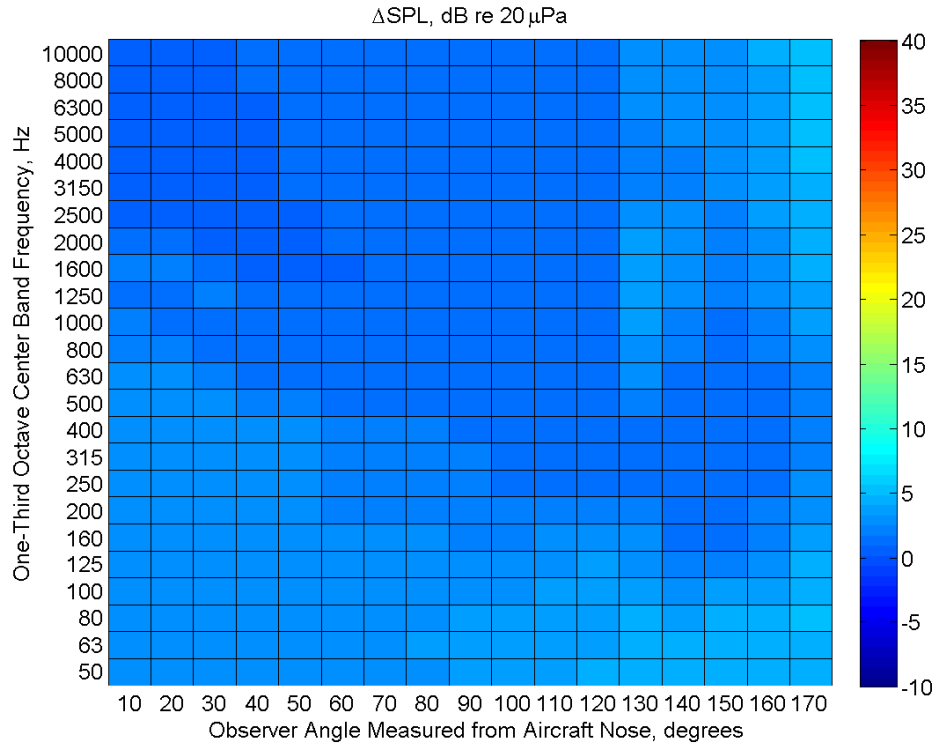With the dominance of the airframe noise at high altitude descent, the approach noise model assumes only airframe noise sources contribute to the received noise. Because the noise generated at low altitude approach, as reflected in the NPD curves currently available in the database, likely contains relative dominance of fan noise, these curves do not represent the noise received from high altitude emission. In this scenario, the engine model cannot be used to predict noise, and a new model is required. The approach noise prediction method was derived from the ANOPP FNKAFM module and, as such, requires several aircraft specific airframe parameters that are currently not available in the AEDT database. Due to the wide variation in these parameters between individual aircraft, it is infeasible to predict approach noise without knowledge of the geometry of the dominant sources of the airframe (i.e. gear, high lift devices, and trailing edge). Because the balance of dominance between these sources varies between specific aircraft, it is also not practical to identify one dominant source to reduce the required input parameter list.

Such geometric data for individual aircraft should be readily available to the FAA from manufacturers, and prediction of high altitude approach noise cannot be performed properly without it. It is thus recommended by the investigators that the AEDT database be expanded to include these parameters (Table 7) for each aircraft.

Assuming these parameters are available, the descent noise prediction at high altitude can be performed. Figure 20 shows the difference in the total noise during descent vs. the airframe noise calculated by the MATLAB script at a distance of 1 ft. for the 150pax model at 18,000 ft. altitude. Neglecting error in frequencies above 1000 Hz, the model predicts the noise very well for all observer angles with a maximum error of 1.9 dBSPL, and an average absolute error of 0.08 dBSPL. All error can be attributed to the fan exhaust noise, and thus the model (slightly) under predicts the ANOPP results.
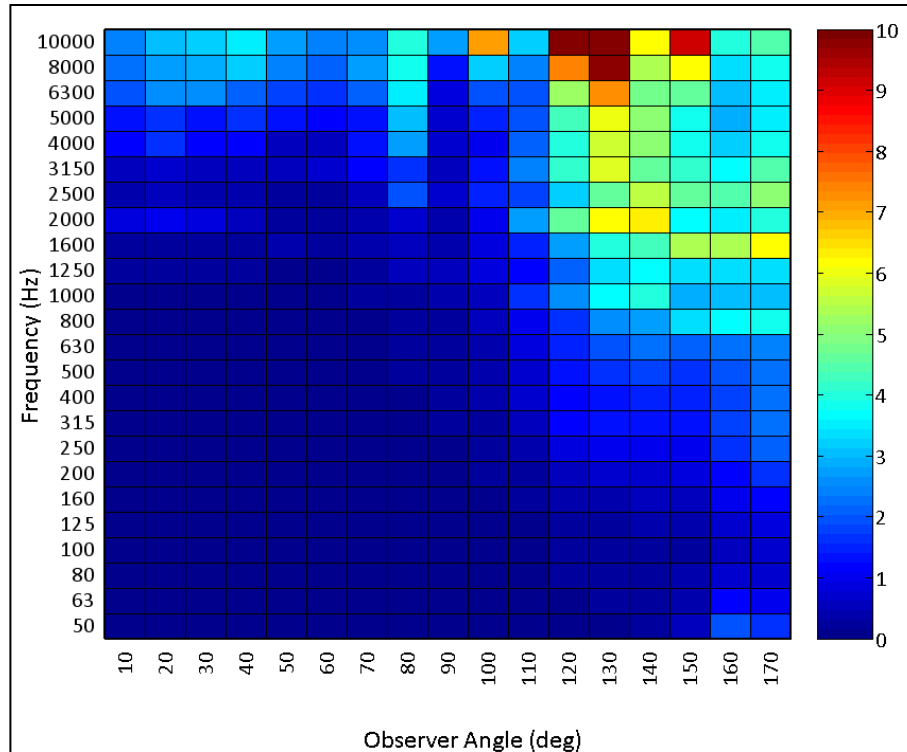
Figure 20: SPL Spectrum Differences for 150pax During Approach

5.0 Potential AEDT Implementation Plan

The first decision in implementing this en route noise prediction method is to decide where to place it. The current Aircraft Acoustics Module (AAM) would be the default choice of placing an implementation of the method described above. Alternatively, a new module could be implemented also. A new module would require replicating much of the required inputs of the AAM and could potentially cause complications in the overall processing flow of AEDT which would require additional logic, especially if this new method is to be seamlessly integrated with the existing methods. If this new method is however only to be used for special analyses and does not require integration with the existing noise prediction method, this could be a feasible implementation and would cleanly separate existing noise prediction methods, which would simplify testing. However, placing the implementation into the AAM would require some modification to the AAM interface, which would impact many other parts of AEDT. Practically, the changes would be relatively limited.

Sections 3.2 and 3.4 described the inputs to the new en route noise prediction method. This section describes how these inputs will be passed from other AEDT modules to an implementation of this method alongside with and implementation of the atmospheric propagation method that is required to compute the final noise at ground receivers.

The primary inputs required are ambient atmospheric parameters. These are available from the Aircraft Performance Module (APM) results or the weather module, which are already

passed to the AAM. The next parameter is the net thrust. This will require an implementation change in the APM to provide noise thrust results for segments computed with the BADA method, since this is the method used for cruise conditions. The remainder of the required inputs is either aircraft specific parameters or parameters that can be derived from a combination of ambient conditions and aircraft specific parameters. The aircraft specific number of engines should be simple but is not. For certain aircraft the number of engines used for the existing noise implementation can vary from the number of engines used in the BADA implementation due to the use of substitutions where no data is available. The recommendation here is that the number of engines is taken from the BADA data, since this will be most consistent with the APM provided data. This implies that a future implementation of this new method will not use existing noise substitutions, but rely on the existing BADA substitutions for potential missing aircraft. At this point it is unclear if this is desirable or appropriate and will have to be investigated if this substitution method is sufficient.

The primary aircraft parameters that are currently not used in the noise computations are FPR, BPR, OPR. Fortunately, BPR and OPR are already provided in the ICAO Engine emissions Databank (EEDB). This means that an implementation of the en route noise method if it uses the already existing data will introduce a dependency with the emissions specific data and therefore complicate possible substitutions a great deal. The only parameter currently not provided anywhere in the AEDT Fleet database is the fan pressure ratio. This parameter will have to be obtained elsewhere and also require and additional column in the fleet database. The most logical location would be to add this column to the FLT_ENGINES table since this is where OPR and BPR currently reside. However, this table currently consists of data from the ICAO EEDB and supplemental data from other sources like EPA or manufacturer data for non ICAO certified engines. This is clearly indicated by the presence or absence of data in the ICAO_UID column. Adding external data in a new column might therefore create consistency problems due to the recursive nature of the EEDB in which entries can be superseded by new test data contained in additional entries. Furthermore, the supplemental data is mostly lacking BPR and OPR data also. Methods describing how the necessary FPR data could be created are contained in [**Error! Bookmark not defined.**] also.

The final implementation design choice to be made is how the results of the en route noise method are used. If the results are intended to exist separately from the results of the existing AAM outputs, they can be simply treated by separate functionality. However, if there is a requirement where both terminal aircraft noise and en route aircraft noise have to be combined into higher level acoustic metrics, the results of this method have to be fully integrated with the existing AAM outputs and also the Acoustic Metrics Module (AMM) inputs and outputs, such that the different types of noise can be combined properly.

The en route noise method is split into three distinct phases. They are en route climb, cruise, and en route descent. The en route climb and cruise phases should follow the method outlined above. The en route descent phase has to follow a different method. This is due to the fact that noise during descent is dominated by airframe noise and should therefore be modeled by airframe specific parameters. Therefore, it is important that any implementation of this method reconcile the engine specific parameters, the airframe specific parameters, and phase of flight dependent application of the method in such a way that potential conflicts due to over or under specification are avoided.

6.0 Conclusion

The cruise source noise is modeled well by the MATLAB script and the current AEDT data. With enhancements to the FPR calculation through the relationship with fan diameter, the error seen in initial results has been minimized. This method was extended to climb noise above 18,000 ft., and care was taken to ensure that the assumption that jet noise was dominant still holds for this condition. With current turbofan engines, the model works well. However, as BPR increases with advanced engine concepts, the jet noise will be reduced, and the assumption may no longer hold.

The descent source noise above 18,000 ft. is also predicted well if all parameters are available. Enhancing the AEDT database to include all relevant airframe geometry data, while no small undertaking, should be a doable task assuming the data easily accessible from manufacturers. Again, the model reflects the current tube and wing aircraft configuration with current engines well, but future concepts may not fit this mold. As the BPR increases with advanced engine concepts, the fan noise may become more dominant at high approach, and this model will need to be modified. Conversely, advanced airframe concepts such as the HWB and the box wing may not be suitably modeled with the ANOPP FNKAFM methodology. While the airframe noise may still be dominant, the prediction method may not accurately reflect the phenomena of advanced concept source noise generation.

With the speed of the algorithm, the model can work well with the rapid analysis goals of AEDT. Future work will involve implementing the algorithm into AEDT as well as enhancing the AEDT database to include the necessary airframe geometry data. In addition, modifications to the model may be required as aircraft that deviate from the tube and wing/turbofan configuration enter the fleet. High fidelity modeling of these concepts is already underway at Georgia Tech within the EDS environment, and rapid, low-fidelity modeling may be possible through adaptation of those efforts.

7.0   Appendix A: Low Order Engine Code Algorithm

7.1 On Design Algorithm

This section will detail the algorithm used to calculate the on design conditions for each engine in the different passenger classes. Much of the algorithm that follows was taken from John Mattingly's *Elements of Propulsion: Gas Turbines and Rockets*. Table 10 gives the inputs variables and the calculated variables needed to perform the on design analysis, a description of their meaning, units, and whether they are a tuning, design, or calculated parameter. A tuning parameter is a parameter that can be changed by the user to force model outputs to match known data, in this case EDS nozzle performance at sea level and en route. Design parameters are parameters either given by AEDT, or unknown parameters that must be estimated, such as FPR. Calculated parameters are outputs resulting from running the model.

Table 10: Nomenclature Table

Variable	Description	Type	Units
OPR	Overall Pressure Ratio	Design	
FPR	Fan Pressure Raito	Design	
BPR	Bypass Ratio	Design	
Altitude	Design altitude in feet	Design	feet
M	Design Mach	Design	
Thrust	Design Thrust in lb$_f$	Design	lb$_f$
ΔT	Difference in temperature from ambient in Rankine	Design	Rankine
ξc	Adiabatic compressor efficiency	Tuning	
ξ_t	Adiabatic turbine efficiency	Tuning	
ξ_f	Adiabatic fan efficiency	Tuning	
ξ_{burner}	Adiabatic burner efficiency	Tuning	
$\xi_{mechanical}$	Mechanical efficiency	Tuning	
π_{burner}	Pressure ratio of the burner	Tuning	
π_{nozzle}	Pressure ratio of the core nozzle	Tuning	
π_{fan}	Pressure ratio of the fan nozzle	Tuning	
π_d	Pressure ratio of the diffuser	Tuning	
γ_c	Specific heat ratio of the compressor	Tuning	
γ_t	Specific heat ratio of the turbine	Tuning	
c_{pc}	Specific heat of the compressor	Tuning	BTU/(lb^{o}F)
c_{pt}	Specific heat of the turbine	Tuning	BTU/(lb^{o}F)
T_{t4}	Maximum Total temperature of the combustor	Tuning	Rankine
h_f	Lower heating value of the fuel	Design	BTU/(lb)
c_f	Cooling factor of bleed flows	Tuning	
CPR	Compressor Pressure Ratio	Calculated	
$T_{ambient}$	Ambient Temperature (Flow station 1)	Calculated	Rankine

Variable	Description	Type	Units
$p_{ambient}$	Ambient pressure (Flow station 1)	Calculated	psia
R_c	Gas constant of the compressor	Calculated	ft*lb$_f$/(lb$_m$*Rankine)
R_t	Gas constant of the turbine	Calculated	ft*lb$_f$/(lb$_m$*Rankine)
a_0	Speed of sound	Calculated	ft/sec
V_0	Velocity of the ambient freestream	Calculated	ft/sec
τ_r	Total Temperature ratio due to ram drag (Station 2/Station 1)	Calculated	
π_r	Total Pressure ratio due to ram drag (Station 2/Station1)	Calculated	
τ_λ	Temperature ratio of total combustor to ambient (Station 4/Station1)	Calculated	
τ_c	Total Temperature ratio of the compressor (Station 3/Station 2)	Calculated	
τ_f	Total Temperature ratio of the fan (Station 12/ Station 1)	Calculated	
f	Overall Fuel to air ratio	Calculated	
τ_t	Total Temperature ratio of the turbine (Station 4/Station 5)	Calculated	
π_t	Total Pressure Ratio of the turbine (Station 4/Station 5)	Calculated	
$\dfrac{p_{t19}}{p_{ambient}}$	Pressure ratio of the total pressure of the bypass nozzle to ambient (Station 19/Station 1)	Calculated	
$\dfrac{T_{t19}}{T_{ambient}}$	Total Temperature ratio of the bypass nozzle to ambient (Station 19/Station 1)	Calculated	
$\dfrac{p_{t9}}{p_{ambient}}$	Pressure ratio of the total pressure of the core nozzle to ambient (Station 9/Station 1)	Calculated	
$\dfrac{T_{t9}}{T_{ambient}}$	Total Temperature ratio of the core nozzle to ambient (Station 9/Station 1)	Calculated	
$\dfrac{p_{t19}}{p_{19}}$	Ratio of total pressure to the static pressure of the bypass nozzle	Calculated	
p_{19}	Static pressure of the bypass nozzle	Calculated	psia
$\dfrac{p_{t9}}{p_9}$	Ratio of the total pressure to the static pressure of the core nozzle	Calculated	
p_9	Static pressure of the core nozzle	Calculated	psia
M_{19}	Mach of the bypass nozzle	Calculated	
$\dfrac{T_{19}}{T_{ambient}}$	Temperature ratio of the bypass nozzle static temperature to the ambient temperature	Calculated	
V_{19}	Bypass nozzle velocity	Calculated	ft/sec
M_9	Core nozzle Mach	Calculated	

Variable	Description	Type	Units
$\dfrac{T_9}{T_{ambient}}$	Temperature ratio of the core nozzle static temperature to the ambient temperature	Calculated	
V_9	Core nozzle velocity	Calculated	ft/sec
p_{t9}	Total pressure of the core nozzle (Station 9)	Calculated	psia
p_{t19}	Total pressure of the bypass nozzle (Station 19)	Calculated	psia
T_{t19}	Total temperature of the core nozzle (Station 19)	Calculated	Rankine
T_{t9}	Total temperature of the bypass nozzle (Station 9)	Calculated	Rankine
T_{sfan}	Static temperature of the bypass nozzle (Station 19)	Calculated	Rankine
T_{score}	Static temperature of the core nozzle (Station 9)	Calculated	Rankine
$\dfrac{F}{\dot{m}}$	Specific Thrust	Calculated	lb$_f$(lb$_m$/s)
$\dot{m}$	Mass flow of the total engine	Calculated	lb$_m$/s
$\dot{m}_{core}$	Mass flow of the core	Calculated	lb$_m$/s
$\dot{m}_{bypass}$	Mass flow of the bypass	Calculated	lb$_m$/s
$TSFC$	Thrust specific fuel consumption	Calculated	
MFP_{19}	Mass flow parameter of the bypass nozzle (Station 19)	Calculated	
MFP_9	Mass flow of the core nozzle (Station 9)	Calculated	
$A9$	Area of the core flow	Calculated	in^2
$A19$	Area of the bypass flow	Calculated	in^2
Variable	Description	Type	Units
OPR$_{on}$	Overall Pressure Ratio for on design	Design	
FPR$_{on}$	Fan Pressure Raito for on design	Design	
BPR$_{on}$	Bypass Ratio for on design	Design	
CPR$_{on}$	Compressor Pressure Ratio for on design	Calculated	
M$_{on}$	Design Mach for on design	Design	
$T_{ambienton}$	Ambient temperature for on design	Calculated	Rankine
$p_{ambienton}$	Ambient pressure for on design	Calculated	Psi
$\dot{m}_{on}$	Mass flow in lb$_m$/s for on design	Calculated	lb$_m$/s
T_{t4on}	Total Temperature of the combustor	Design	Rankine
MFP_{19on}	Mass flow parameter of the bypass for on design	Calculated	
MFP_{9on}	Mass flow parameter of the core for on design	Calculated	
π_t	Turbine pressure ratio for on design	Calculated	

Variable	Description	Type	Units
τ_{ton}	Turbine total temperature for on design	Calculated	
τ_{fon}	Fan total temperature ratio for on design	Calculated	
τ_{con}	Compressor total temperature ratio for on design	Calculated	
A_9	Area of the core flow	Calculated	in^2
A_{19}	Area of the fan flow	Calculated	in^2
OPR	Overall Pressure Ratio	Design	
FPR	Fan Pressure Raito	Design	
BPR	Bypass Ratio	Design	
Altitude	Design altitude	Design	feet
M	Design Mach	Design	
Thrust	Design Thrust	Design	lb_f
ΔT	Difference in temperature from ambient	Design	Rankine
ξc	Adiabatic compressor efficiency	Tuning	
ξ_t	Adiabatic turbine efficiency	Tuning	
ξ_f	Adiabatic fan efficiency	Tuning	
ξ_{burner}	Adiabatic burner efficiency	Design	
$\xi_{mechanical}$	Mechanical efficiency	Tuning	
π_{burner}	Pressure ratio of the burner	Design	
π_{nozzle}	Pressure ratio of the core nozzle	Tuning	
π_{fan}	Pressure ratio of the fan nozzle	Tuning	
π_d	Pressure ratio of the diffuser	Tuning	
γ_c	Specific heat of the compressor	Design	
γ_t	Specific heat of the turbine	Tuning	
c_{pc}	Specific heat of the compressor	Tuning	BTU/(lb^{o}F)
c_{pt}	Specific heat of the turbine	Tuning	BTU/(lb^{o}F)
T_{t4}	Total temperature of the combustor	Design	Rankine
h_f	Heating factor of the engine fuel	Design	BTU/(lb)
c_f	Cooling factor of bleed flows	Tuning	
CPR	Compressor Pressure Ratio	Calculated	
$T_{ambient}$	Ambient Temperature (Flow station 1)	Calculated	Rankine
$p_{ambient}$	Ambient pressure (Flow station 1)	Calculated	psia
R_c	Gas constant of the compressor	Calculated	ft*lb$_f$/(lb$_m$*Rankine)
R_t	Gas constant of the turbine	Calculated	ft*lb$_f$/(lb$_m$*Rankine)
a_0	Speed of sound	Calculated	ft/sec
V_0	Velocity of the engine	Calculated	ft/sec
τ_r	Total Temperature ratio due to ram drag (Station 2/Station 1)	Calculated	
π_r	Total Pressure ratio due to ram drag (Station 2/Station1)	Calculated	
τ_λ	Temperature ratio of total combustor to	Calculated	

Variable	Description	Type	Units
	ambient (Station 4/Station1)		
τ_c	Total Temperature ratio of the compressor (Station 3/Station 2)	Calculated	
τ_f	Total Temperature ratio of the fan (Station 12/ Station 1)	Calculated	
f	Fuel to air ratio	Calculated	
τ_t	Total Temperature ratio of the turbine (Station 4/Station 5)	Calculated	
π_t	Total Pressure Ratio of the turbine (Station 4/Station 5)	Calculated	
$\dfrac{p_{t19}}{p_{ambient}}$	Pressure ratio of the total pressure of the bypass nozzle to ambient (Station 19/Station 1)	Calculated	
$\dfrac{T_{t19}}{T_{ambient}}$	Total Temperature ratio of the bypass nozzle to ambient (Station 19/Station 1)	Calculated	
$\dfrac{p_{t9}}{p_{ambient}}$	Pressure ratio of the total pressure of the core nozzle to ambient (Station 9/Station 1)	Calculated	
$\dfrac{T_{t9}}{T_{ambient}}$	Total Temperature ratio of the core nozzle to ambient (Station 9/Station 1)	Calculated	
$\dfrac{p_{t19}}{p_{19}}$	Ratio of total pressure to the static pressure of the bypass nozzle	Calculated	
p_{19}	Static pressure of the bypass nozzle	Calculated	psia
$\dfrac{p_{t9}}{p_9}$	Ratio of the total pressure to the static pressure of the core nozzle	Calculated	
p_9	Static pressure of the core nozzle	Calculated	psia
M_{19}	Mach of the bypass nozzle	Calculated	
$\dfrac{T_{19}}{T_{ambient}}$	Temperature ratio of the bypass nozzle static temperature to the ambient temperature	Calculated	
V_{19}	Bypass nozzle velocity	Calculated	ft/sec
M_9	Core nozzle Mach	Calculated	
$\dfrac{T_9}{T_{ambient}}$	Temperature ratio of the core nozzle static temperature to the ambient temperature	Calculated	
V_9	Core nozzle velocity	Calculated	ft/sec
p_{t9}	Total pressure of the core nozzle (Station 9)	Calculated	psia
p_{t19}	Total pressure of the bypass nozzle (Station 19)	Calculated	psia
T_{t19}	Total temperature of the core nozzle (Station 19)	Calculated	Rankine

Variable	Description	Type	Units
T_{t9}	Total temperature of the bypass nozzle (Station 9)	Calculated	Rankine
T_{sfan}	Static temperature of the bypass nozzle (Station 19)	Calculated	Rankine
T_{score}	Static temperature of the core nozzle (Station 9)	Calculated	Rankine
$\dfrac{F}{\dot{m}}$	Specific Thrust	Calculated	lb$_f$(lb$_m$/s)
$\dot{m}$	Mass flow of the total engine	Calculated	lb$_m$/s
$\dot{m}_{core}$	Mass flow of the core	Calculated	lb$_m$/s
$\dot{m}_{bypass}$	Mass flow of the bypass	Calculated	lb$_m$/s
$TSFC$	Thrust specific fuel consumption	Calculated	
MFP_{19}	Mass flow parameter of the bypass nozzle (Station 19)	Calculated	
MFP_9	Mass flow of the core nozzle (Station 9)	Calculated	
BPR	Bypass Ratio	Calculated	
$Thrust$	Thrust of the engine	Calculated	lb$_f$
$Thrust$	Thrust of the engine	Calculated	lb$_f$
$\dfrac{p_{t19}}{p_{ambient}}$	Pressure ratio of the total pressure of the bypass nozzle to ambient (Station 19/Station 1)	Calculated	
$\dfrac{p_{t9}}{p_{ambient}}$	Pressure ratio of the total pressure of the core nozzle to ambient (Station 9/Station 1)	Calculated	
$\dfrac{T_{t19}}{T_{ambient}}$	Total Temperature ratio of the bypass nozzle to ambient (Station 19/Station 1)	Calculated	
$\dfrac{T_{t9}}{T_{ambient}}$	Total Temperature ratio of the core nozzle to ambient (Station 9/Station 1)	Calculated	

To better understand the nomenclature of the following equations. Figure 21 gives flow station designations of a typical turbofan engine.
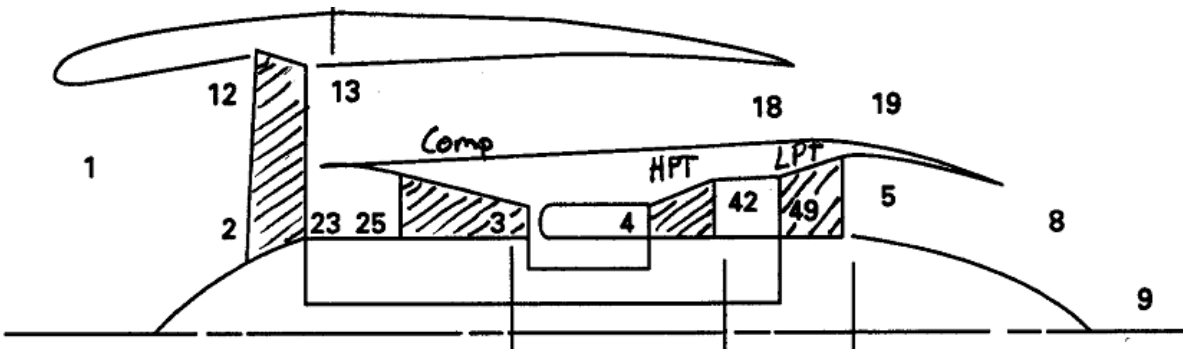

Figure 21: Flow Station Designations for Typical Turbofan Engine

First, the compressor pressure ratio was calculated by the following equation

$$CPR = \frac{OPR}{FPR} \tag{2}$$

To find the ambient temperature and pressure for the given flight conditions, the altitude had to be checked. The following equations give the ambient temperature and pressure as a function of the altitude the aircraft is flying at. It should be noted that the temperature is in degrees Rankine and the pressure is in pounds per square inch.

$$if\ altitude < 36089$$

$$T_{ambient} = \big((59 + \Delta Temperature) - .00356616 altitude\big) + 460 \tag{3}$$

$$p_{ambient} = 14.69(1 - 6.875 \cdot 10^{-6} \cdot altitude)^{5.2561} \tag{4}$$

$$else$$

$$T_{ambient} = (-69.7 + \Delta Temperature) + 460 \tag{5}$$

$$p_{ambient} = 14.69\left(.2234 e^{-\frac{(altitude - 36089)}{20806.7}}\right) \tag{6}$$

Once these conditions were known, the cycles of the engine could be cycled through using the following equations.

$$R_c = 778.16 c_{pc} \frac{\gamma_c - 1}{\gamma_c} \tag{7}$$

$$R_t = 778.16 c_{pt} \frac{\gamma_t - 1}{\gamma_t} \tag{8}$$

$$a_0 = \sqrt{32.2\gamma_c R_c T_{ambient}} \tag{9}$$

$$V_0 = a_0 M \tag{10}$$

$$\tau_r = 1 + \frac{\gamma_c - 1}{2} M^2 \tag{11}$$

$$\pi_r = \tau_r^{1.4/(1.4-1)} \tag{12}$$

$$\tau_\lambda = \frac{c_{pt} T_{t4}}{c_{pc} T_{ambient}} \tag{13}$$

$$\tau_c = 1 + \frac{1}{\xi_c}(CPR^{\gamma_c-1/\gamma_c} - 1) \tag{14}$$

$$\tau_f = 1 + \frac{1}{\xi_f}(FPR^{\gamma_c-1/\gamma_c} - 1) \tag{15}$$

$$f = \frac{\tau_\lambda - \tau_r\tau_c}{\left(\xi_{burner}h_f/c_{pc}T_{ambient}\right) - \tau_\lambda} \tag{16}$$

$$\tau_t = 1 - \frac{1}{(1+f)\xi_{mechanical}}\frac{\tau_r}{\tau_\lambda}\left(\tau_c - 1 + c_fBPR(\tau_f - 1)\right) \tag{17}$$

$$\pi_t = (1 - \frac{1}{\xi_t}(1 - \tau_t))^{\gamma_t/(\gamma_t-1)} \tag{18}$$

$$\frac{p_{t19}}{p_{ambient}} = \pi_r\pi_dFPR\pi_{fan} \tag{19}$$

$$\frac{T_{t19}}{T_{ambient}} = \tau_r\tau_f \tag{20}$$

$$\frac{p_{t9}}{p_{ambient}} = \pi_r\pi_dFPR \cdot CPR\pi_{burner}\pi_t\pi_{nozzle} \tag{21}$$

$$\frac{T_{t9}}{T_{ambient}} = \frac{\tau_tT_{t4}}{T_{ambient}} \tag{22}$$

Both the fan nozzle and the core nozzle had to be checked to see if they were chocked, and the following logic was used to see if they were chocked and to calculate the engine parameters that were dependent upon them being chocked or not. A flow diagram of this process is shown in Figure 22, and the equations are given afterwards.
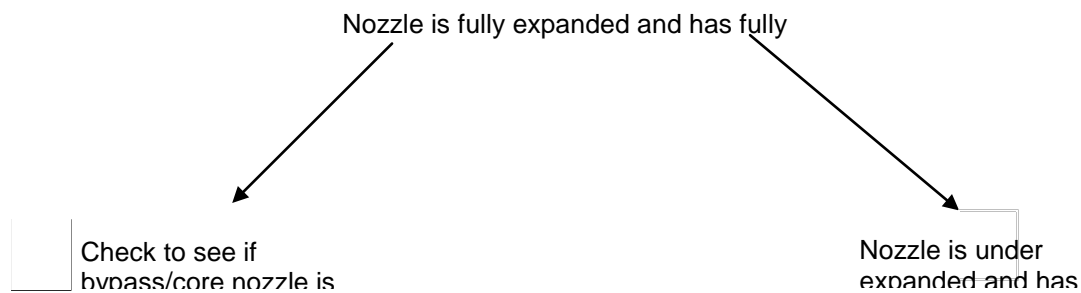
Nozzle is fully expanded and has fully

Check to see if
bypass/core nozzle is

Nozzle is under
expanded and has

Figure 22: Logic for Nozzle Exit Pressure Conditions

$$if \frac{p_{t19}}{p_{ambient}} < \left(\frac{\gamma_c + 1}{2}\right)^{\gamma_c/(\gamma_c-1)}$$

$$\frac{p_{t19}}{p_{19}} = \frac{p_{t19}}{p_{ambient}} \tag{23}$$

$$p_{19} = p_{ambient} \tag{24}$$

$$else$$

$$\frac{p_{t19}}{p_{19}} = \left(\frac{\gamma_c+1}{2}\right)^{\gamma_c/(\gamma_c-1)} \tag{25}$$

$$p_{19} = \left(\frac{\frac{p_{t19}}{p_{19}}}{\left(\frac{\gamma_c+1}{2}\right)^{\gamma_c/(\gamma_c-1)}}\right) p_{ambient} \tag{26}$$

$$if \frac{p_{t9}}{p_{ambient}} < \left(\frac{\gamma_t + 1}{2}\right)^{\gamma_t/(\gamma_t-1)}$$

$$\frac{p_{t9}}{p_9} = \frac{p_{t9}}{p_{ambient}} \tag{27}$$

$$p_9 = p_{ambient} \tag{28}$$

$$else$$

$$\frac{p_{t9}}{p_9} = \left(\frac{\gamma_t+1}{2}\right)^{\gamma_t/(\gamma_t-1)} \tag{29}$$

$$p_9 = \left(\frac{\frac{p_{t9}}{p_9}}{\left(\frac{\gamma_t+1}{2}\right)^{\gamma_t/(\gamma_t-1)}}\right) p_{ambient} \tag{30}$$

$$M_{19} = \sqrt{\frac{2}{\gamma_c-1}\left[\left(\frac{p_{t19}}{p_{19}}\right)^{(\gamma_c-1)/\gamma_c} - 1\right]} \tag{31}$$

$$\frac{T_{19}}{T_{ambient}} = \frac{\tau_r \tau_f}{\left(\frac{p_{t19}}{p_{19}}\right)^{(\gamma_c-1)/\gamma_c}} \tag{32}$$

$$\frac{V_{19}}{a_0} = M_{19}\sqrt{\frac{T_{19}}{T_{ambient}}} \tag{33}$$

$$V_{19} = a_0 M_{19}\sqrt{\frac{T_{19}}{T_{ambient}}} \tag{34}$$

$$M_9 = \sqrt{\frac{2}{\gamma_t - 1}\left[\left(\frac{p_{t9}}{p_9}\right)^{(\gamma_t - 1)/\gamma_t} - 1\right]} \tag{35}$$

$$\frac{T_9}{T_{ambient}} = \frac{\tau_\lambda \tau_t c_{pc}}{\left(c_{pt}\left(\frac{p_{t9}}{p_9}\right)^{(\gamma_t - 1)/\gamma_t}\right)} \tag{36}$$

$$\frac{V_9}{a_0} = M_9\sqrt{\frac{T_9}{T_{ambient}}\frac{\gamma_t R_t}{\gamma_c R_c}} \tag{37}$$

$$V_9 = a_0 M_9\sqrt{\frac{T_9}{T_{ambient}}\frac{\gamma_t R_t}{\gamma_c R_c}} \tag{38}$$

$$p_{t9} = \frac{p_{t9}}{p_{ambient}}p_{ambient} \tag{39}$$

$$p_{t19} = \frac{p_{t19}}{p_{ambient}}p_{ambient} \tag{40}$$

$$T_{t19} = \tau_r \tau_f T_{ambient} \tag{41}$$

$$T_{t9} = \tau_t T_{t4} \tag{42}$$

$$T_{sfan} = \frac{\left(\frac{T_{19}}{T_{ambient}}\right)T_{ambient}}{1 + \frac{.4}{2}M_{19}^2} \tag{43}$$

$$T_{score} = \frac{\left(\frac{T_9}{T_{ambient}}\right)T_{ambient}}{1 + \frac{.33}{2}M_9^2} \tag{44}$$

$$\frac{F}{\dot{m}} = \frac{1}{1+BPR}\frac{a_0}{32.2}\left((1+f)\frac{V_9}{a_0} - M + (1+f)\frac{R_t}{R_c}\frac{T_{score}/T_{ambient}}{\frac{V_9}{a_0}}\frac{1 - p_{ambient}/p_9}{\gamma_t}\right) +$$
$$\frac{BPR}{1+BPR}\frac{a_0}{32.2}\left(\frac{V_{19}}{a_0} - M + \frac{T_{fan}/T_{ambient}}{\frac{V_{19}}{a_0}}\frac{1 - p_{ambient}/p_{19}}{\gamma_c}\right) \tag{45}$$

$$\dot{m} = \frac{Thrust}{\frac{F}{\dot{m}}} \tag{46}$$

$$\dot{m}_{core} \frac{\dot{m}}{1+BPR} \tag{47}$$

$$\dot{m}_{bypass} = BPR\dot{m}_{core} \tag{48}$$

$$TSFC = 3600 \left(\frac{f/((1+BPR)c_f)}{\frac{F}{\dot{m}}} \right) \tag{49}$$

$$MFP_{19} = \left(1 - \frac{\gamma_c - 1}{2} M_{19}{}^2 \right)^{\gamma_c+1/2(\gamma_c-1)} M_{19} \sqrt{\frac{32.2\gamma_c}{R_c}} \tag{50}$$

$$MFP_9 = \left(1 - \frac{\gamma_t - 1}{2} M_9{}^2 \right)^{\gamma_t+1/2(\gamma_t-1)} M_9 \sqrt{\frac{32.2\gamma_t}{R_t}} \tag{51}$$

$$A_{19} = \frac{\dot{m}_{bypass} \sqrt{\left(\frac{T_{19}}{T_{ambient}}\right) T_{ambient}}}{MFP_{19}\left(\frac{p_{t19}}{p_{ambient}}\right) p_{ambient}} \tag{52}$$

$$A_9 = \frac{\dot{m}_{core} \sqrt{\left(\frac{T_9}{T_{ambient}}\right) T_{ambient}}}{MFP_9\left(\frac{p_{t9}}{p_{ambient}}\right) p_{ambient}} \tag{53}$$

7.2 Off Design Algorithm

This section will detail the algorithm used to calculate the engine off design parameters for a given engine type and passenger class. As with the on design algorithm, much of this process is taken from Mattingly's *Elements of Propulsion: Gas Turbines and Rockets*. An iterative technique is necessary to solve the equations for conservation of mass and energy that dictate the engine operation away from the design conditions. The momentum equation is typically not carried for steady state calculations.

To begin the iteration, the fan conditions and the turbine conditions are set to those found for the on design case. The turbine and fan conditions are then recalculated using the appropriate equations, and the turbine pressure ratio is checked to see if it is within the limit of

error. Essentially, the program is guessing at the work output of the turbine, calculating the resulting work input and mass flow through the compressor, and iterating until a closed solution is found. If for some reason the code does not converge it usually indicates a non-physical operating condition. A flow diagram of the algorithm's iteration process is shown in Figure 7. The process for this algorithm was taken from Mattingly's *Elements of Propulsion: Gas Turbines and Rockets.*
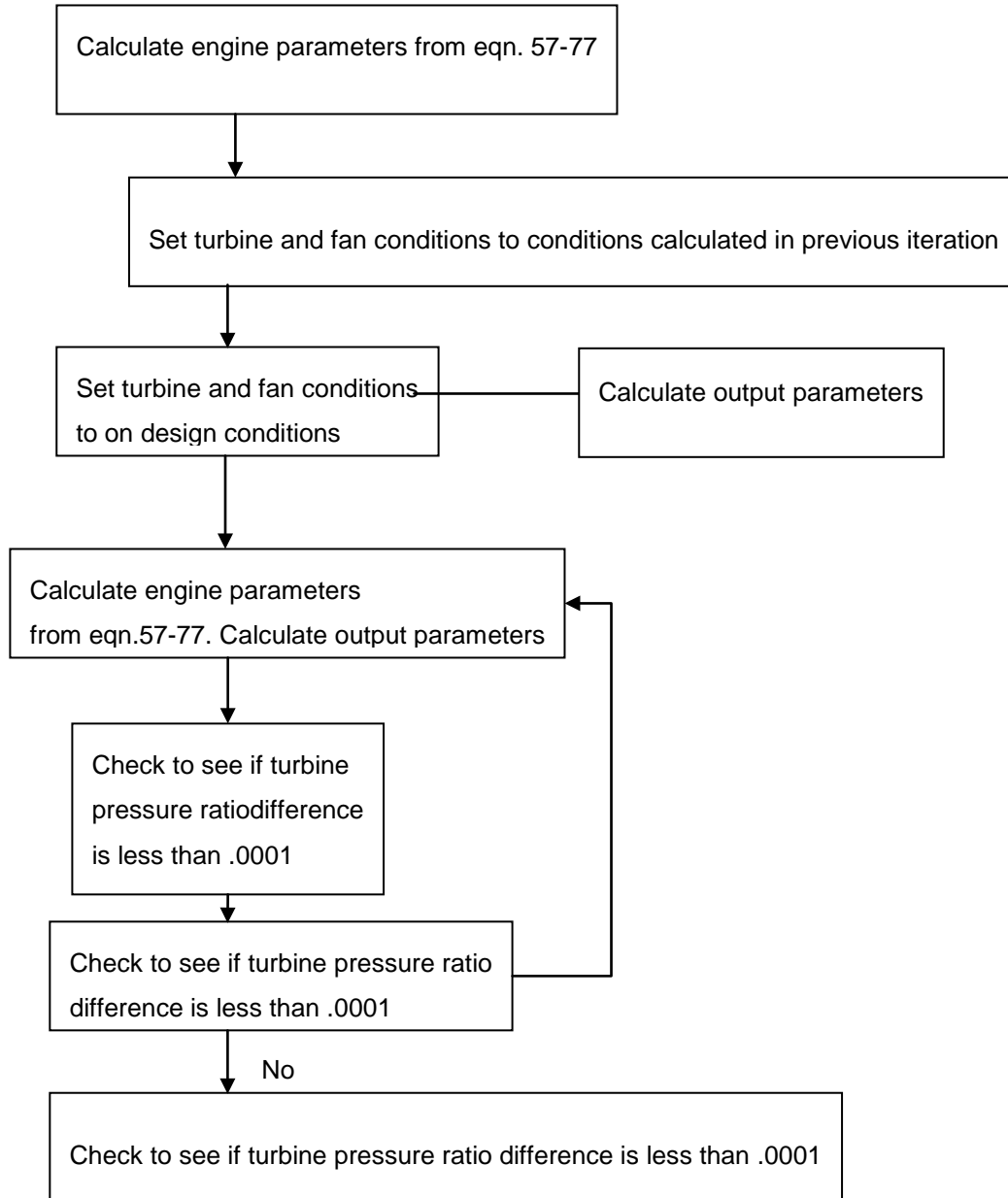
```
┌─────────────────────────────────────────────┐
│ Calculate engine parameters from eqn. 57-77  │
└─────────────────────────────────────────────┘
                      │
                      ▼
┌────────────────────────────────────────────────────────────────┐
│ Set turbine and fan conditions to conditions calculated in      │
│ previous iteration                                              │
└────────────────────────────────────────────────────────────────┘
                      │
                      ▼
┌──────────────────────────────┐        ┌──────────────────────────┐
│ Set turbine and fan conditions├───────│ Calculate output parameters│
│ to on design conditions       │        └──────────────────────────┘
└──────────────────────────────┘
                      │
                      ▼
┌──────────────────────────────────────┐
│ Calculate engine parameters           │◄──────────┐
│ from eqn.57-77. Calculate output      │           │
│ parameters                            │           │
└──────────────────────────────────────┘           │
                      │                             │
                      ▼                             │
┌──────────────────────────────┐                   │
│ Check to see if turbine        │                  │
│ pressure ratiodifference       │                  │
│ is less than .0001             │                  │
└──────────────────────────────┘                   │
                      │                             │
                      ▼                             │
┌──────────────────────────────────────┐           │
│ Check to see if turbine pressure ratio │──────────┘
│ difference is less than .0001          │
└──────────────────────────────────────┘
                      │ No
                      ▼
┌──────────────────────────────────────────────────────────────┐
│ Check to see if turbine pressure ratio difference is less than .0001 │
└──────────────────────────────────────────────────────────────┘
```

Figure 23: Off Design Algorithm Flow Diagram

As with the off design case, the ambient temperature, ambient pressure, R_c, and R_t are given by equations 6 and 7. The τ_r and τ_λ for both the on design case and the off design case is calculated by equations 10 and 12. The off design algorithm is an iterative process, and the

following equations are used to set up the iterative process. Note that the subscript '*on*' denotes the design value of a particular parameter.

$$\tau_t = \tau_{ton} \tag{54}$$

$$\tau_f = \tau_{fon} \tag{55}$$

$$\pi_t = \pi_{ton} \tag{56}$$

$$\tau_c = 1 + \frac{\tau_\lambda / \tau_r}{\tau_{\lambda on} / \tau_{ron}} \frac{\tau_f}{\tau_{fon}} (\tau_{con} - 1) \tag{57}$$

$$CPR = (1 + (\tau_c - 1)\xi_c)^{\gamma_c / (\gamma_c - 1)} \tag{58}$$

$$FPR = (1 + (\tau_f - 1)\xi_f)^{\gamma_c / (\gamma_c - 1)} \tag{59}$$

$$\frac{p_{t19}}{p_{ambient}} = \pi_r \pi_d FPR \pi_{fan} \tag{60}$$

$$\frac{p_{t9}}{p_{ambient}} = \pi_r \pi_d FPR \cdot CPR \pi_{burner} \pi_t \pi_{nozzle} \tag{61}$$

$$if \; \frac{p_{t19}}{p_{ambient}} < \left(\frac{\gamma_c + 1}{2}\right)^{\gamma_c / (\gamma_c - 1)}$$

$$\frac{p_{t19}}{p_{19}} = \frac{p_{t19}}{p_{ambient}} \tag{62}$$

$$p_{19} = p_{ambient} \tag{63}$$

$$else$$

$$\frac{p_{t19}}{p_{19}} = \left(\frac{\gamma_c + 1}{2}\right)^{\gamma_c / (\gamma_c - 1)} \tag{64}$$

$$p_{19} = \left(\frac{\frac{p_{t19}}{p_{19}}}{\left(\frac{\gamma_c + 1}{2}\right)^{\gamma_c/(\gamma_c-1)}} \right) p_{ambient} \qquad (65)$$

$$if \; \frac{p_{t9}}{p_{ambient}} < \left(\frac{\gamma_t + 1}{2}\right)^{\gamma_t/(\gamma_t-1)}$$

$$\frac{p_{t9}}{p_9} = \frac{p_{t9}}{p_{ambient}} \qquad (66)$$

$$p_9 = p_{ambient} \qquad (67)$$

$$else$$

$$\frac{p_{t9}}{p_9} = \left(\frac{\gamma_t + 1}{2}\right)^{\gamma_t/(\gamma_t-1)} \qquad (68)$$

$$p_9 = \left(\frac{\frac{p_{t9}}{p_9}}{\left(\frac{\gamma_t + 1}{2}\right)^{\gamma_t/(\gamma_t-1)}} \right) p_{ambient} \qquad (69)$$

$$M_{19} = \sqrt{\frac{2}{\gamma_c - 1}\left[\left(\frac{p_{t19}}{p_{19}}\right)^{(\gamma_c-1)/\gamma_c} - 1\right]} \qquad (70)$$

$$M_9 = \sqrt{\frac{2}{\gamma_t - 1}\left[\left(\frac{p_{t9}}{p_9}\right)^{(\gamma_t-1)/\gamma_t} - 1\right]} \qquad (71)$$

$$MFP_{19} = \left(1 - \frac{\gamma_c - 1}{2}M_{19}^2\right)^{\gamma_c+1/2(\gamma_c-1)} M_{19}\sqrt{\frac{32.2\gamma_c}{R_c}} \qquad (72)$$

$$MFP_9 = \left(1 - \frac{\gamma_t - 1}{2} M_9{}^2\right)^{\gamma_t+1/2(\gamma_t-1)} M_9 \sqrt{\frac{32.2\gamma_t}{R_t}} \tag{73}$$

$$BPR = BPR_{on} \frac{CPR_{on}/FPR_{on}}{CPR/FPR} \frac{MFP_{19}}{MFP_{19on}} \sqrt{\frac{\tau_\lambda/(\tau_r\tau_f)}{\tau_{\lambda on}/(\tau_{ron}\tau_{fon})}} \tag{74}$$

$$\tau_{fnew} = 1 + (\tau_{fon} - 1)\frac{1 - \tau_t}{1 - \tau_{ton}} \frac{\tau_\lambda/(\tau_r)}{\tau_{\lambda on}/(\tau_{ron})} \frac{1 + BPR}{1 + BPR_{on}} \tag{75}$$

$$\tau_{tnew} = 1 - \xi_t \left(1 - \pi_t{}^{(\gamma_t-1)/\gamma_t}\right) \tag{76}$$

$$\pi_{tnew} = \pi_{ton} \frac{MFP_{9on}}{MFP_9} \sqrt{\frac{\pi_{tnew}}{\pi_{ton}}} \tag{77}$$

$$\delta = |\pi_t - \pi_{tnew}| \tag{78}$$

The algorithm then iterates until δ is less than .0001. The τ_{fnew}, τ_{tnew}, and π_{tnew} from the previous step become the τ_f, τ_t, and π_t of the next step. The algorithm also has a counter that keeps track of how many iterations the algorithm has performed and exits if the count is above 25. Once the iterations have finished, the following equations are used to find the final set of output data. Note if the counter was too high, all of these values are set to 999 so that the user knows that the convergence failed. This output data consists of the nozzle operating conditions which can be used to find thrust and are subsequently entered into the shock cell prediction calculations.

$$\tau_t = \tau_{tnew} \tag{79}$$

$$\tau_f = \tau_{fnew} \tag{80}$$

$$\pi_t = \pi_{tnew} \tag{81}$$

$$\tau_c = 1 + \frac{\tau_\lambda/\tau_r}{\tau_{\lambda on}/\tau_{ron}}\frac{\tau_f}{\tau_{fon}}(\tau_{con} - 1) \tag{82}$$

$$CPR = (1 + (\tau_c - 1)\xi_c)^{\gamma_c/(\gamma_c-1)} \tag{83}$$

$$FPR = (1 + (\tau_f - 1)\xi_f)^{\gamma_c/(\gamma_c-1)} \tag{84}$$

$$\frac{p_{t19}}{p_{ambient}} = \pi_r\pi_d FPR\pi_{fan} \tag{85}$$

$$\frac{p_{t9}}{p_{ambient}} = \pi_r\pi_d FPR \cdot CPR\pi_{burner}\pi_t\pi_{nozzle} \tag{86}$$

$$if\, \frac{p_{t19}}{p_{ambient}} < \left(\frac{\gamma_c + 1}{2}\right)^{\gamma_c/(\gamma_c-1)}$$

$$\frac{p_{t19}}{p_{19}} = \frac{p_{t19}}{p_{ambient}} \tag{87}$$

$$p_{19} = p_{ambient} \tag{88}$$

$$else$$

$$\frac{p_{t19}}{p_{19}} = \left(\frac{\gamma_c + 1}{2}\right)^{\gamma_c/(\gamma_c-1)} \tag{89}$$

$$p_{19} = \left(\frac{\frac{p_{t19}}{p_{19}}}{\left(\frac{\gamma_c + 1}{2}\right)^{\gamma_c/(\gamma_c-1)}}\right)p_{ambient} \tag{90}$$

$$if\, \frac{p_{t9}}{p_{ambient}} < \left(\frac{\gamma_t + 1}{2}\right)^{\gamma_t/(\gamma_t-1)} \tag{91}$$

$$\frac{p_{t9}}{p_9} = \frac{p_{t9}}{p_{ambient}} \tag{92}$$

$$p_9 = p_{ambient} \tag{93}$$

$$\textit{else}$$

$$\frac{p_{t9}}{p_9} = \left(\frac{\gamma_t + 1}{2}\right)^{\gamma_t/(\gamma_t-1)} \tag{94}$$

$$p_9 = \left(\frac{p_{t9}}{p_9} \middle/ \left(\frac{\gamma_t + 1}{2}\right)^{\gamma_t/(\gamma_t-1)}\right) p_{ambient} \tag{95}$$

$$M_{19} = \sqrt{\frac{2}{\gamma_c - 1}\left(\frac{p_{t19}}{p_{19}}\right)^{(\gamma_c-1)/\gamma_c}} \tag{96}$$

$$M_9 = \sqrt{\frac{2}{\gamma_t - 1}\left(\frac{p_{t9}}{p_9}\right)^{(\gamma_t-1)/\gamma_t}} \tag{97}$$

$$MFP_{19} = \left(1 - \frac{\gamma_c - 1}{2}M_{19}{}^2\right)^{\gamma_c+1/2(\gamma_c-1)} M_{19}\sqrt{\frac{32.2\gamma_c}{R_c}} \tag{98}$$

$$MFP_9 = \left(1 - \frac{\gamma_t - 1}{2}M_9{}^2\right)^{\gamma_t+1/2(\gamma_t-1)} M_9\sqrt{\frac{32.2\gamma_t}{R_t}} \tag{99}$$

$$BPR = BPR_{on}\frac{CPR_{on}/FPR_{on}}{CPR/FPR}\frac{MFP_{19}}{MFP_{19on}}\sqrt{\frac{\tau_\lambda/(\tau_r\tau_f)}{\tau_{\lambda on}/(\tau_{ron}\tau_{fon})}} \tag{100}$$

$$\frac{T_{t19}}{T_{ambient}} = \tau_r\tau_f \tag{101}$$

$$\frac{T_{t9}}{T_{ambient}} = \frac{\tau_t T_{t4}}{T_{ambient}} \tag{102}$$

$$\frac{T_{19}}{T_{ambient}} = \frac{\tau_r \tau_f}{\left(\frac{p_{t19}}{p_{19}}\right)^{(\gamma_c - 1)/\gamma_c}} \tag{103}$$

$$\frac{V_{19}}{a_0} = M_{19}\sqrt{\frac{T_{19}}{T_{ambient}}} \tag{104}$$

$$V_{19} = a_0 M_{19}\sqrt{\frac{T_{19}}{T_{ambient}}} \tag{105}$$

$$\frac{T_9}{T_{ambient}} = \frac{\tau_\lambda \tau_c c_{pc}}{\left(c_{pt}\left(\frac{p_{t9}}{p_9}\right)^{(\gamma_c - 1)/\gamma_c}\right)} \tag{106}$$

$$\frac{V_9}{a_0} = M_9\sqrt{\frac{T_9}{T_{ambient}}\frac{\gamma_t R_t}{\gamma_c R_c}} \tag{107}$$

$$V_9 = a_0 M_9\sqrt{\frac{T_9}{T_{ambient}}\frac{\gamma_t R_t}{\gamma_c R_c}} \tag{108}$$

$$T_{sfan} = \frac{\left(\frac{T_{19}}{T_{ambient}}\right)T_{ambient}}{1 + \frac{.4}{2}M_{19}^2} \tag{109}$$

$$T_{score} = \frac{\left(\frac{T_9}{T_{ambient}}\right)T_{ambient}}{1 + \frac{.33}{2}M_9^2} \tag{110}$$

$$\frac{F}{\dot{m}} = \frac{1}{1+BPR}\frac{a_0}{32.2}\left((1+f)\frac{V_9}{a_0} - M + (1\right.$$

$$\left. + f)\frac{R_t}{R_c}\frac{T_{score}/T_{ambient}}{\frac{V_9}{a_0}}\frac{1 - p_{ambient}/p_9}{\gamma_t}\right)$$

$$+ \frac{BPR}{1+BPR}\frac{a_0}{32.2}\left(\frac{V_{19}}{a_0} - M + \frac{T_{fan}/T_{ambient}}{\frac{V_{19}}{a_0}}\frac{1 - p_{ambient}/p_{19}}{\gamma_c}\right) \qquad (111)$$

$$p_{t9} = \frac{p_{t9}}{p_{ambient}}p_{ambient} \qquad (112)$$

$$p_{t19} = \frac{p_{t19}}{p_{ambient}}p_{ambient} \qquad (113)$$

$$T_{t19} = \tau_r\tau_f T_{ambient} \qquad (114)$$

$$T_{t9} = \tau_t T_{t4} \qquad (115)$$

$$OPR = CPR \cdot FPR \qquad (116)$$

$$\dot{m} = \dot{m}_{on}\frac{1+BPR_{on}}{1+BPR}\frac{\pi_r\pi_d FPR \cdot CPRp_{ambient}}{\pi_{ron}\pi_{don}FPR_{on} \cdot CPR_{on}p_{ambienton}}\sqrt{\frac{T_{t4on}}{T_{t4}}} \qquad (117)$$

$$\dot{m}_{core}\frac{\dot{m}}{1+BPR} \qquad (118)$$

$$\dot{m}_{bypass} = BPR\dot{m}_{core} \qquad (119)$$

$$f = \frac{\tau_\lambda - \tau_r\tau_f\tau_c}{h_f\xi_b/c_{pc}T_{ambient} - \tau_\lambda} \qquad (120)$$

$$Thrust = \dot{m}\frac{F}{\dot{m}} \qquad (121)$$

7.3 Complete Calibration Results

The following graphics show core and bypass nozzle pressure and temperature ratio for cruise segments at Mach 0.8, 35,000 feet, and climb segments for the different passenger classes using the cycle data from EDS combined with the tuning parameters shown in Table 3.
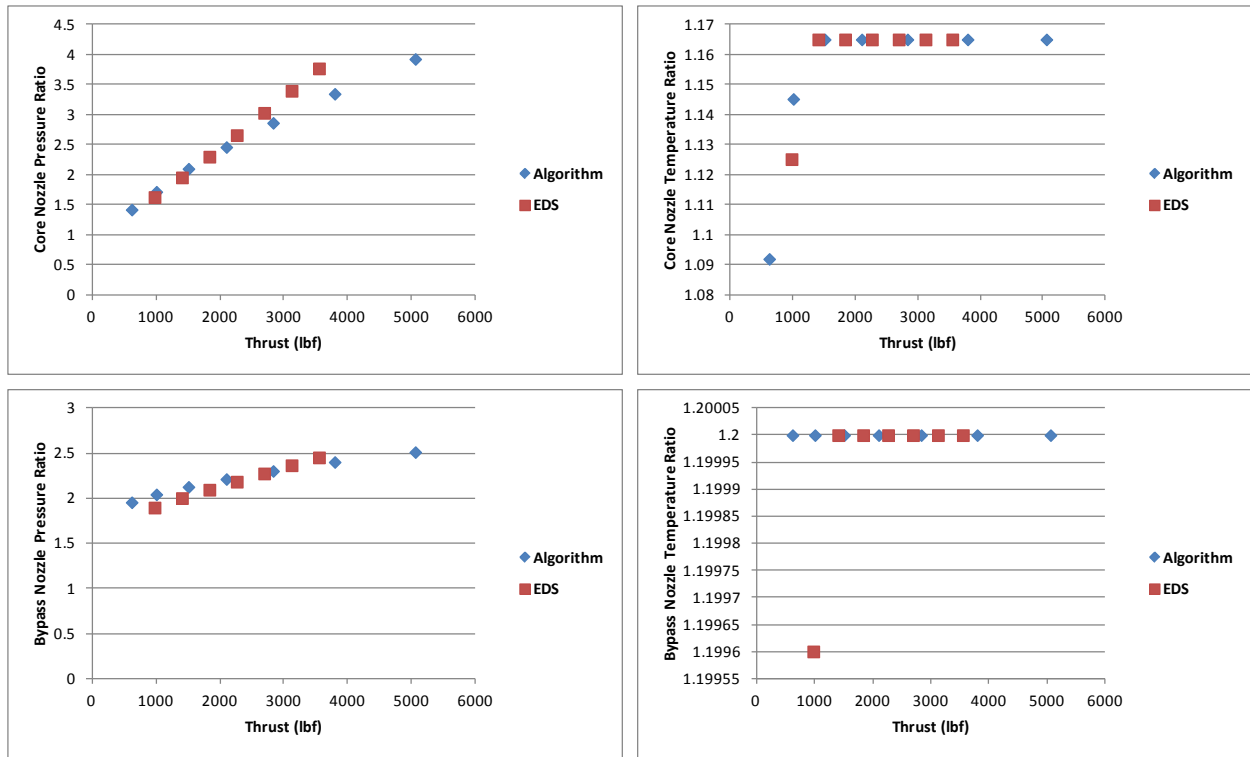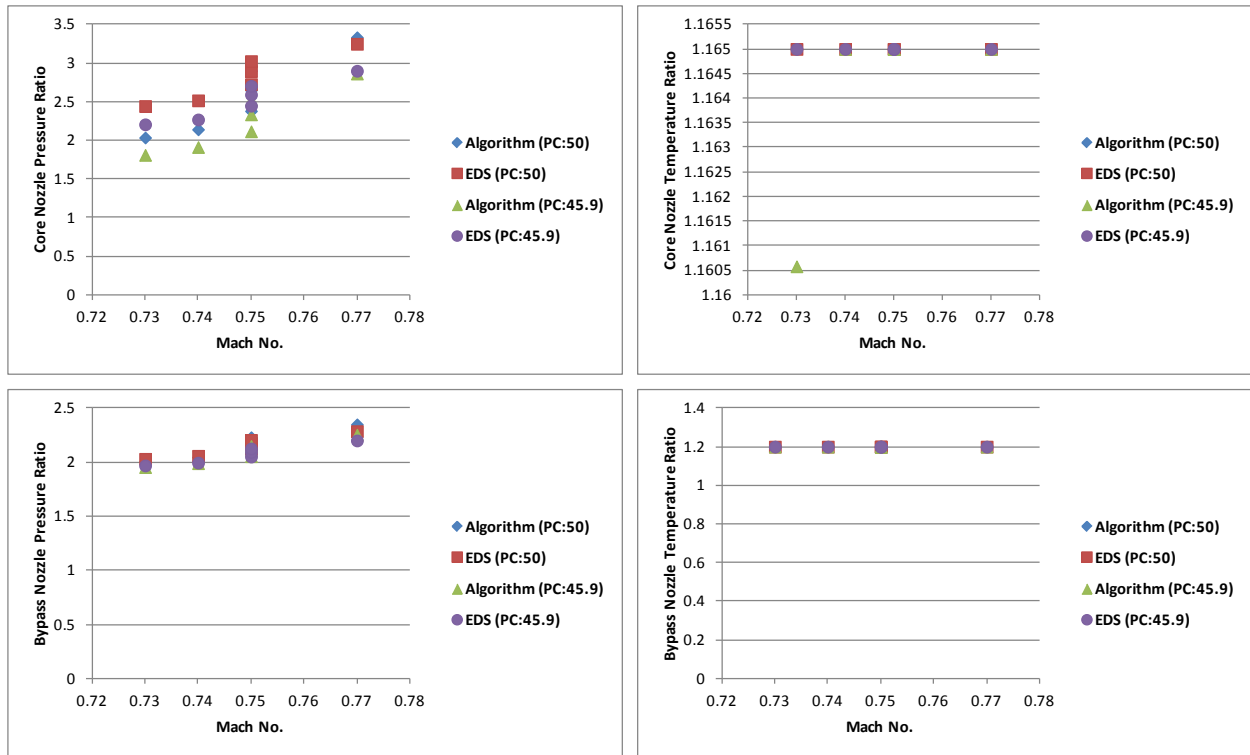
Figure 24: 50PAX Cruise Values
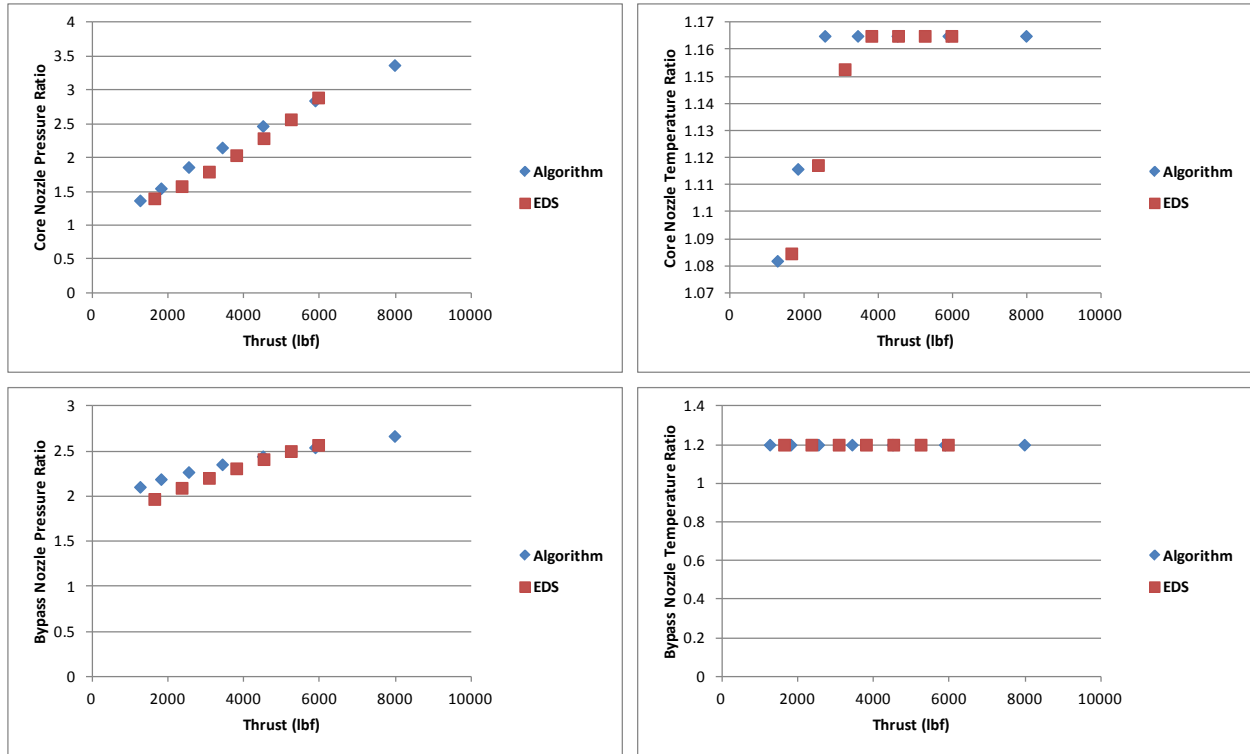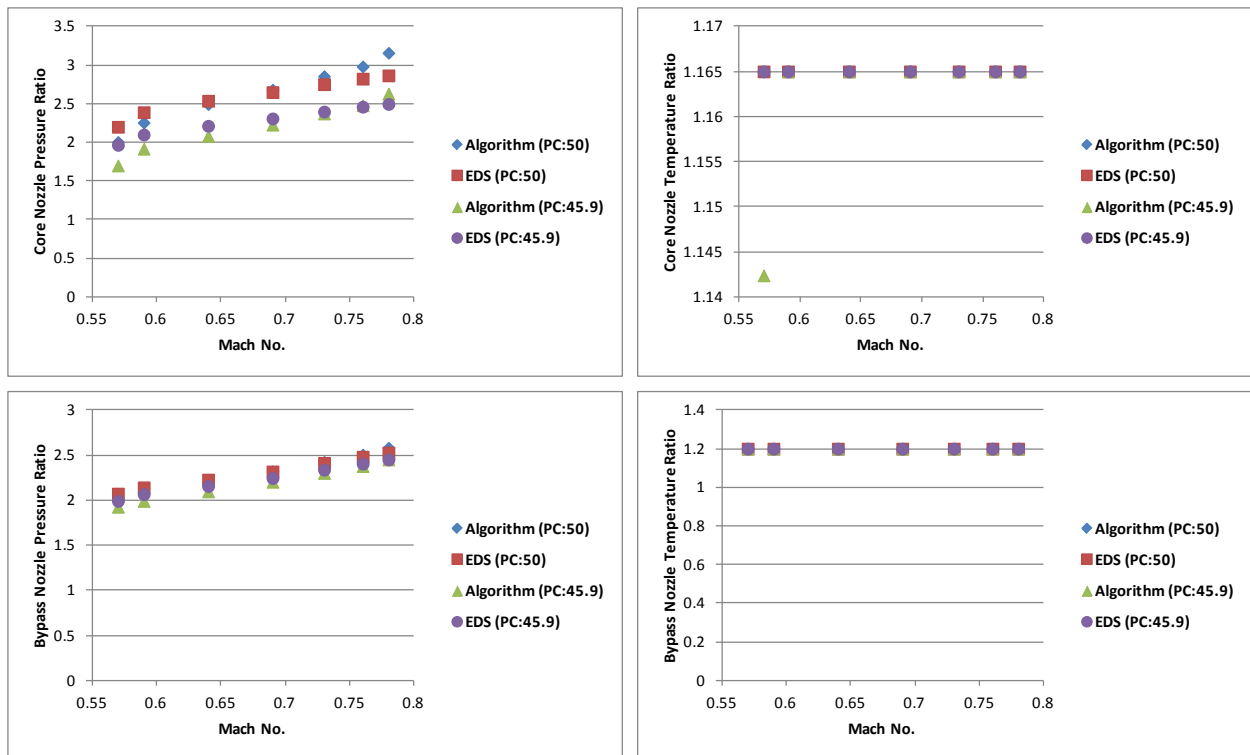

Figure 25: 50PAX Climb Values

Figure 30: 150PAX Cruise Values

Figure 31: 150PAX Climb Values
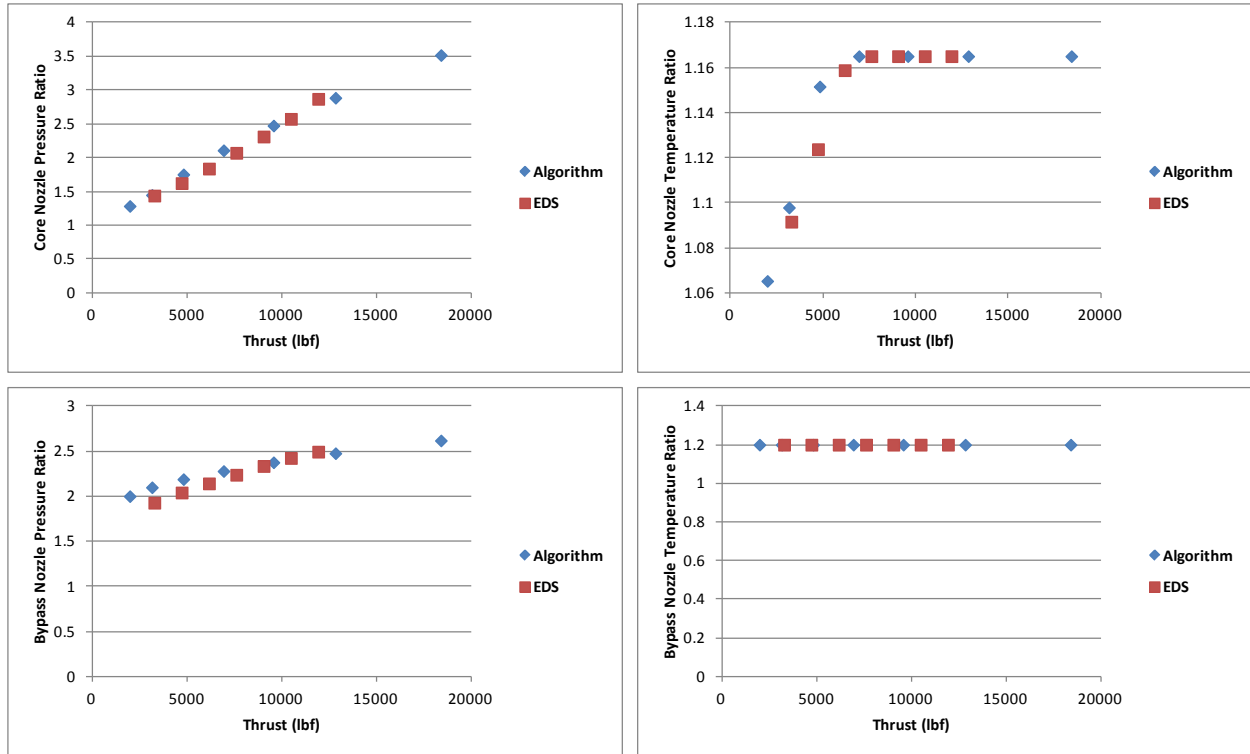
Figure 32: 210PAX Cruise Values
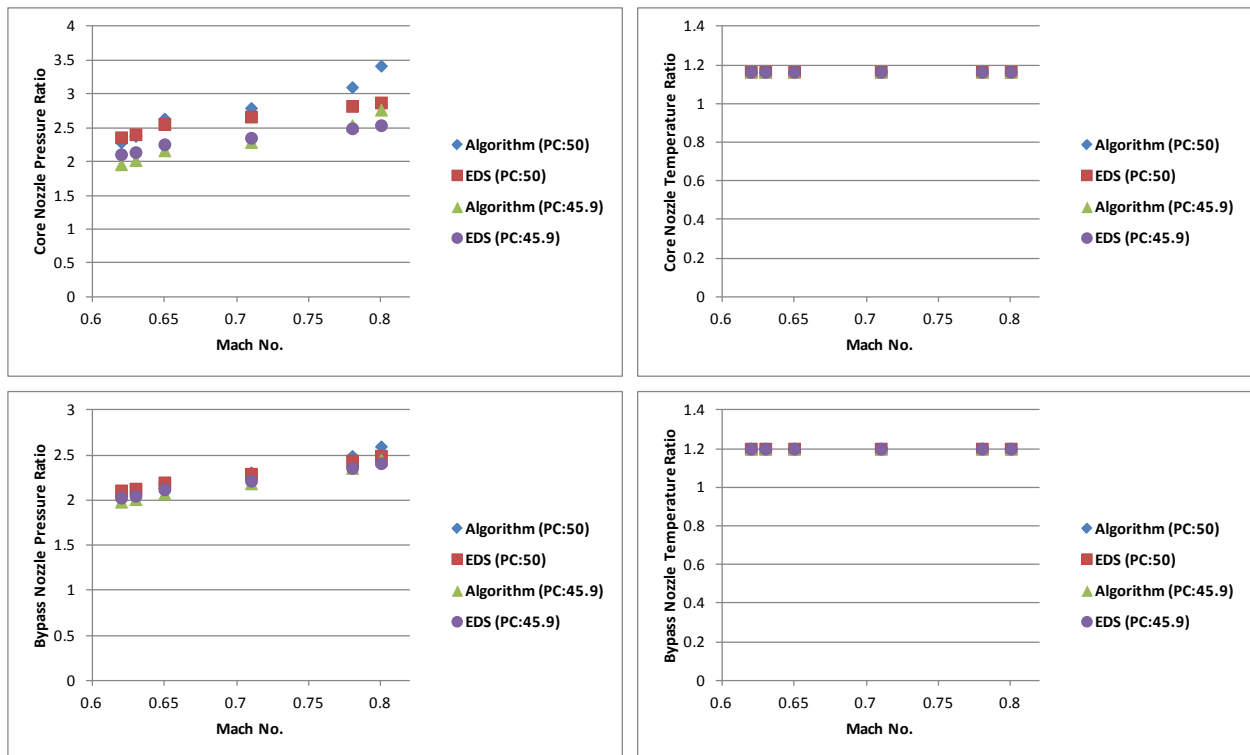
Figure 33: 210PAX Climb Values
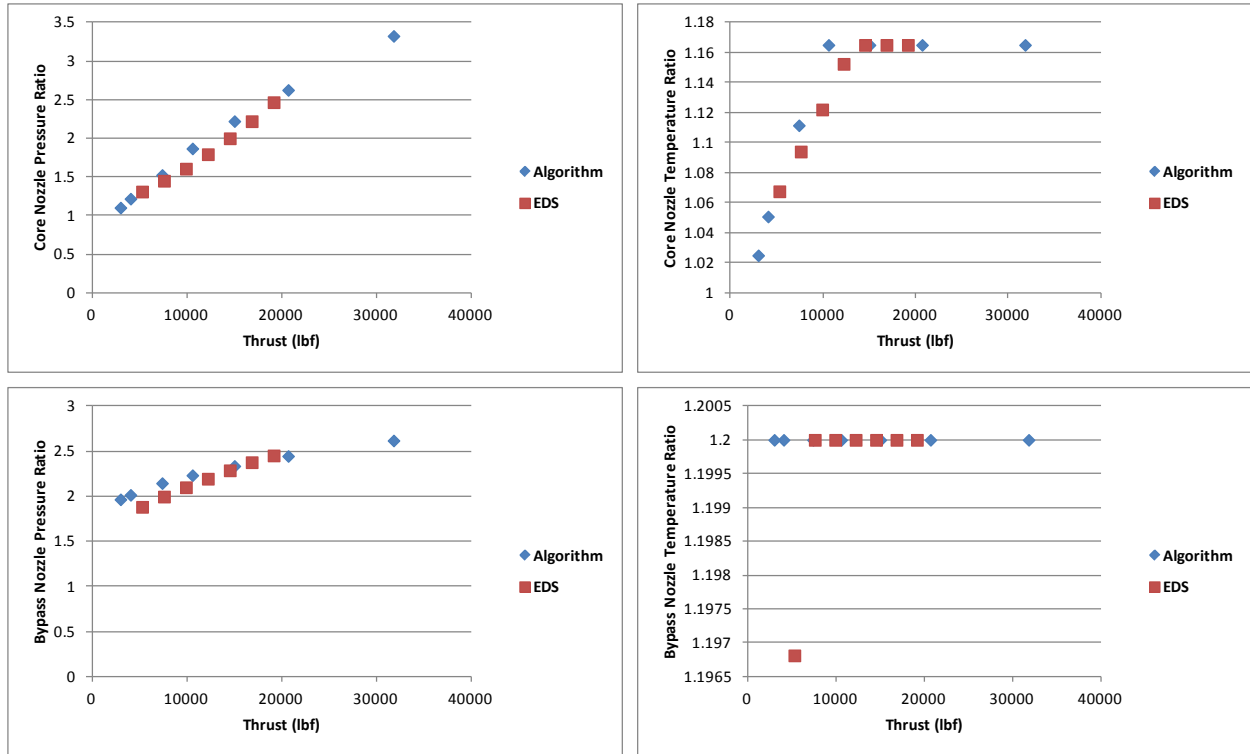
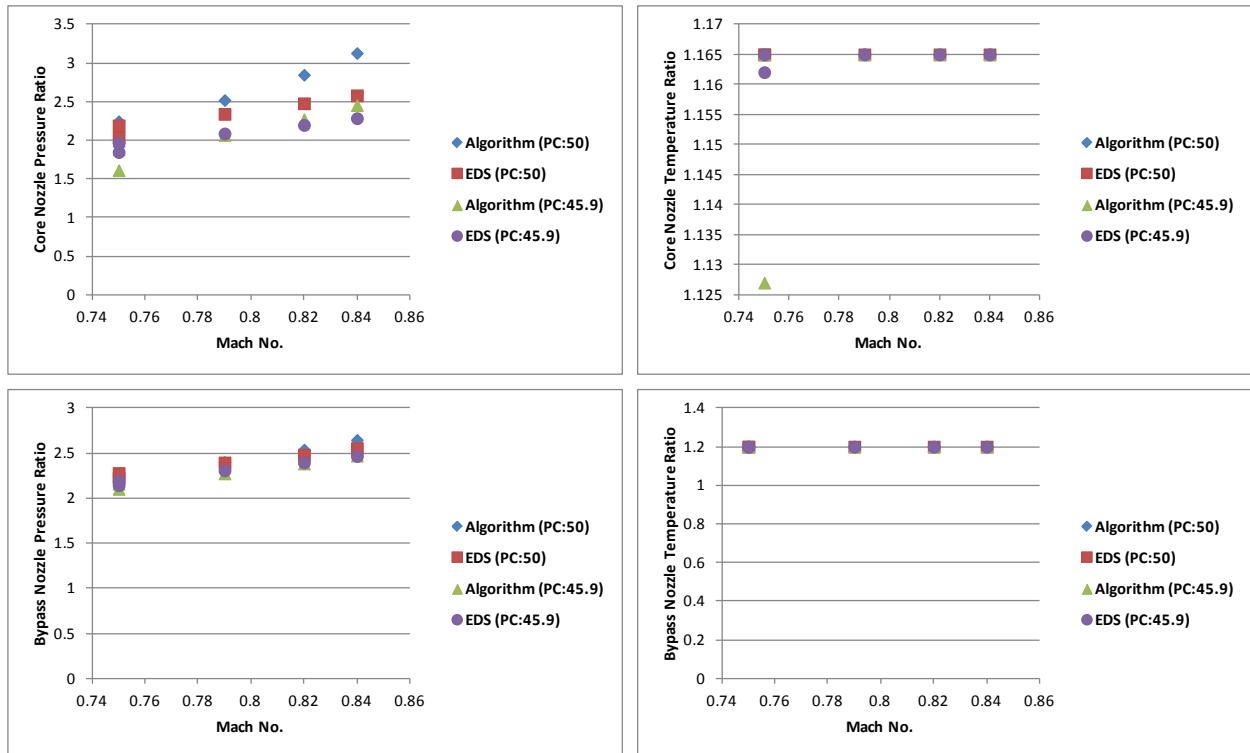**Figure 34: 300PAX Cruise Values**

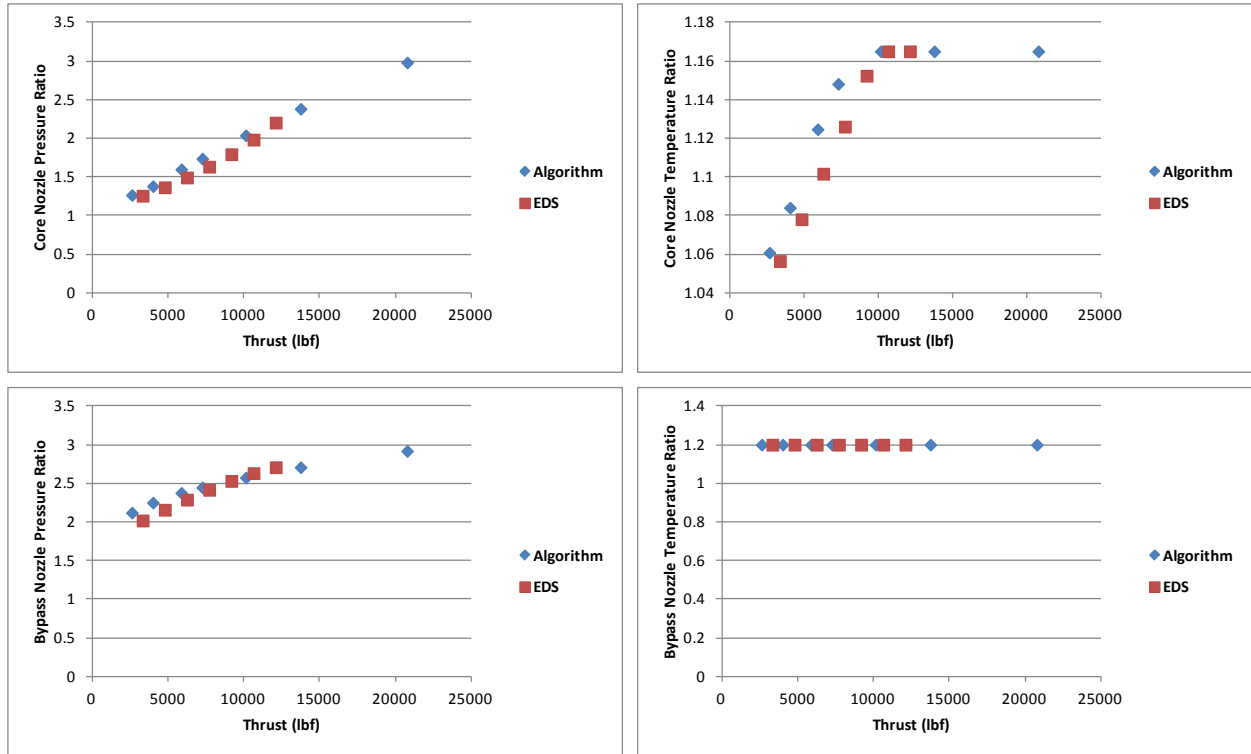
Figure 35: 300PAX Climb Values

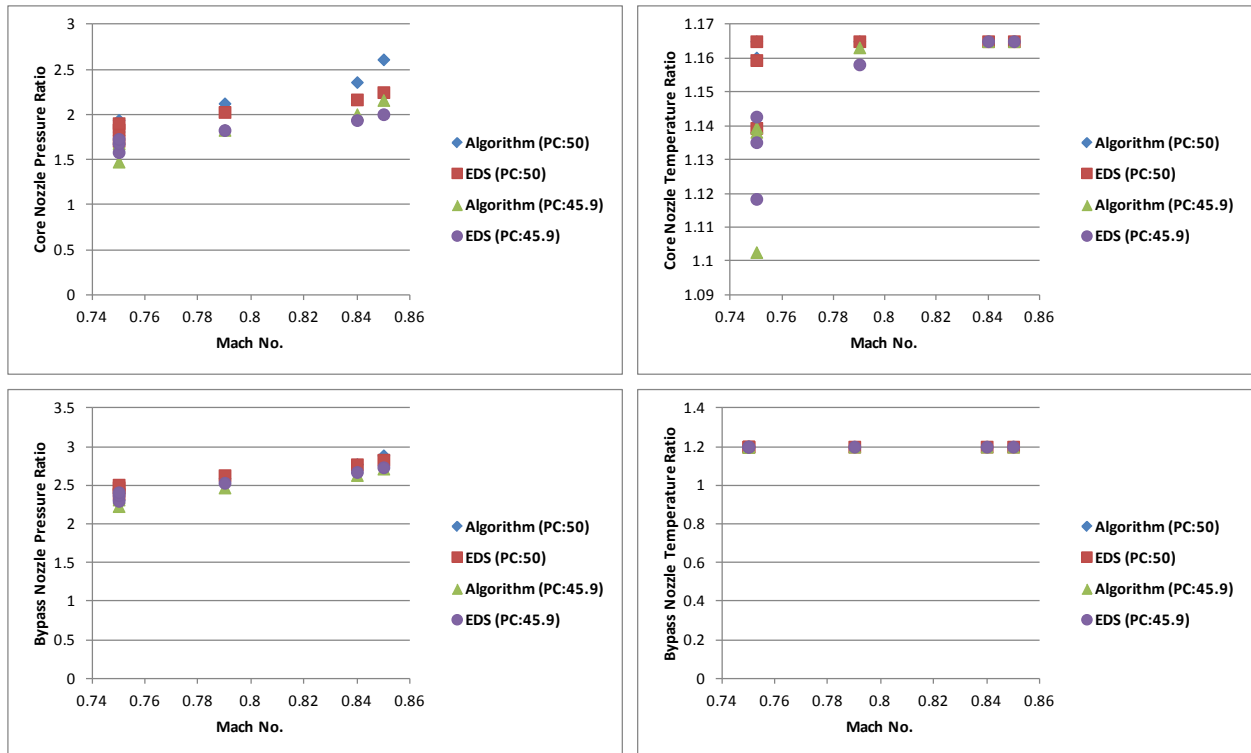**Figure 36: 400PAX Cruise Values**

Figure 37: 400PAX Climb Values

8.0 References

[1] Lytle, J., 1999. The Numerical Propulsion System Simulation: A Multidisciplinary Design for Aerospace Vehicles. Tech. Rep. NASA TM-1999-209194, September.

[2] Lytle, J., 2000. The Numerical Propulsion System Simulation: An Overview. Tech. Rep. NASA TM-2000-209915, June.

[3] Converse, G., and Giffin, R., 1984. Extended Parametric Representation of Compressors Fans and Turbines. Vol. I -CMGEN User's Manual. Tech. Rep. NASA CR-174645, March.

[4] Onat, E., and Klees, G., 1979. A Method to Estimate Weight and Dimensions of Large and Small Gas Turbine Engines. Tech. Rep. NASA-CR-159481, January.

[5] Schutte, J., "Simultaneous Multi-Design Point Approach to Gas Turbine On-Design Cycle Analysis for Aircraft Engines," Ph.D. Thesis, School of Aerospace Engineering, Georgia Institute of Technology, May 2009.

[6] McCullers, L. Flight Optimization System, Release 8.11, User's Guide, Revised 9 October 2009.

[7] Zorumski, W. "Aircraft Noise Prediction Program theoretical Manual, Part 1" NASA TM-83199-Pt-1, February 1982.

[8] Zorumski, W. "Aircraft Noise Prediction Program theoretical Manual, Part 2" NASA TM-83199-Pt-2, February 1982.

[9] Gliebe, P., "Noise vs. Correctd Thrust Evaluation in SAE AIR 1845 – Additional Analysis," SAE A21 General Meeting, Nov. 2-4, 2004.

[10] "Aircraft Noise Prediction Program Theoretical Manual." NASA TM 83199 Part 1, November 2008.

[11] Hay, J.A., and Rose, E.G., "In-Flight Shock Cell Boise," Journal of Sound and Vibration, Apr., 1970.